

---

**Faculty of Mechanical  
Science  
and Engineering**

**Institute of Process  
Engineering and  
Environmental  
Technology**

---

**Chair of Transport  
Process at Interfaces**

## **Research Project**

# **Numerical Simulation of Electrical Conductivity in Liquid Foams**

submitted in fulfillment of the requirements for the degree “Master of Science”

<b>Name</b>	Smita Ashokrao Salunkhe
<b>Born on</b>	7. January 1999
<b>Place of birth</b>	Maharashtra, India
<b>Submission date</b>	12. September 2025
<b>Examiner</b>	Dr.-Ing. Sascha Heitkam
<b>Supervisor</b>	Dr.-Ing. Artem Skrypnik

## Module CMS-PRO - Research Project

The regular processing time for project work and written project report is 16 weeks. After the project report has been submitted, the oral presentation takes place as arranged between the examiner and the student.

*To be completed by the student:*

Full Name: Smita Ashokrao Salunkhe Student ID: 5185721

Study: M.Sc. Computational Modeling and Simulation

Track: Computational Engineering

Start Date: 1/6/25 End Date: 30/9/25

Topic: Numerical simulation of Electrical Conductivity in Liquid Foams

Task description:

The primary objective of this research project is to perform numerical simulations of the electrical conductivity of liquid foams exhibiting isotropic and anisotropic structures. The project involves developing numerical models from raw data and comparing the simulation results with established theoretical models.

Supervisor: Dr. Artem Skrypnik  
Examiner: Dr. Sascha Heitkam

The module examination consists of a written project report and an oral presentation of 30 minutes, both in English.

23/5/25

Date

22/5/25

Date

23/5/25

Date

Smita Ashokrao  
Salunkhe

Digital signed by Smita Ashokrao  
Salunkhe  
Datum: 2025.05.23 15:45:34 +02'00'

Signature (Student)

Artem Skrypnik Digital signed by Artem Skrypnik  
Datum: 2025.05.22 14:15:35 +02'00'

Signature (Supervisor)

 Digital unterschrieben von Sascha  
Heitkam  
Datum: 2025.05.23 14:18:45 +02'00'

Signature (Examiner)

## Acknowledgements

I am especially grateful to my supervisor, **Dr.-Ing. Artem Skrypnik**, for his encouragement, continuous guidance, and for providing the geometrical data used in this study. I would also like to thank my examiner, **Dr.-Ing. Sascha Heitkam**, for giving me the opportunity to undertake this work and for his valuable feedback. A special thank-you goes to **Dipl.-Ing. Tine Marquardt** for recommending me for this project. Additionally, I would like to express my gratitude to the FWDT team, who, directly or indirectly, contributed to this work and helped me, knowingly or unknowingly. I am grateful to **Marwan Chammouma, PhD student** for providing the tomography data of solidified alginate foams, acquired at the Institut Charles Sadron within the *Théorie et Simulation des Polymères* group (PI: **Dr. Jean Farago**) and the *Mechanics of Interfaces and Multiphase Systems* group (PI: **Dr. Aurélie Hourlier-Fargette**).

I would also like to acknowledge the use of tools such as *Grammarly* and *DeepL* for refining sentence structure and grammar. Additionally, I used *ChatGPT* to aid in understanding and searching for relevant material on the topic, and latex code generation for adding figures in report.

# Abstract

Liquid foams are gas-liquid dispersions with a flexible, highly deformable geometry that provides a large gas-liquid interfacial area. Hence, they have widespread applications in various fields, including cosmetics, cleaning agents, firefighting, insulation, and advanced structural materials. The structure of liquid foam comprises thin films meeting in Plateau borders; the arrangement of these Plateau borders marks whether the foam geometry is structured or unstructured. In this study, a numerical simulation approach is used to investigate the effect of liquid foam geometry on its electrical conductivity. This approach enables the comparison of structured and unstructured geometries and quantification of directional effects. By evaluating relative conductivity at the liquid fractions relevant to each geometry and comparing it with established effective-medium models, it is possible to isolate the role of topology from liquid-fraction effects, assess anisotropy, and examine the sensitivities and uncertainties associated with these effects.

# Contents

<b>1</b>	<b>Introduction</b>	<b>1</b>
1.1	Application and Relevance of Liquid Foams . . . . .	1
1.2	Liquid Foam Structure . . . . .	1
1.2.1	Important Processes In Liquid Foams . . . . .	3
1.2.2	Dry and Wet Foams . . . . .	4
1.2.3	Mechanical Properties of Liquid Foams . . . . .	4
1.3	Electrical Conductivity . . . . .	5
1.4	Solid and Liquid Foams . . . . .	6
1.5	Research Focus . . . . .	7
<b>2</b>	<b>Theoretical Background and State of the Art</b>	<b>8</b>
2.1	Overview of Foam Structure and Transport Properties . . . . .	8
2.2	Electrical Conductivity of Liquid Foams . . . . .	8
2.2.1	Lemlich Model . . . . .	9
2.2.2	Maxwell model . . . . .	10
2.2.3	Empirical relation of Feitosa <i>et al.</i> . . . . .	10
2.3	Role of Microstructure . . . . .	10
2.3.1	Structured Foams . . . . .	10
2.4	Existing Models, Simulation Approaches, and Motivation . . . . .	12
<b>3</b>	<b>Materials and Methods</b>	<b>14</b>
3.1	Geometry Acquisition and Preparation . . . . .	14
3.2	Numerical Framework . . . . .	19
3.2.1	Universal Equations, Governing Equation and Assumptions . . . . .	19
3.2.2	ANSYS-Based FEM Framework . . . . .	21
3.3	Mesh Convergence Study . . . . .	23
3.3.1	Mesh Convergence Study on Single Plateau Border . . . . .	24
3.3.2	Meshing strategy for Full Liquid Foam Geometry . . . . .	25
3.4	PostProcessing . . . . .	26
3.4.1	Validation Approach . . . . .	27
<b>4</b>	<b>Results</b>	<b>28</b>
4.1	Visualization of Results . . . . .	28
4.1.1	Unstructured Foam . . . . .	28
4.1.2	Structured and Unstructured Comparison . . . . .	30

<b>5</b>	<b>Discussion</b>	<b>33</b>
5.1	Unstructured geometry . . . . .	33
5.1.1	Structured versus Unstructured Foam Geometry . . . . .	34
5.1.2	Uncertainty and Sensitivity . . . . .	34
<b>6</b>	<b>Conclusion and Future Work</b>	<b>36</b>

# List of Figures

1.1	Three dimensional visualization of the structure of a liquid foam, showing its key elements: <b>liquid films (lamellae)</b> separating adjacent bubbles, <b>Plateau borders</b> where three films meet, and <b>nodes (vertices)</b> where four Plateau borders converge. . . . .	2
3.1	Tool chain used for geometry preparation, generated using the Microsoft PowerPoint presentation tool. The same workflow was applied to both the single Plateau border and the full foam geometry. . . . .	14
3.2	Workflow of geometry preparation from tomography data: (a) raw grayscale CT slice, (b) After cleaning and Otsu thresholding (4D x 4D size depicted by red dashed box on raw CT image), a binary mask is obtained (0 = air, 1 = material), suitable for 3D reconstruction.(c) Volumetric unstructured liquid foam reconstruction generated by stacking 641 binary slices.The green box at corners highlights the bounding box for mesh and output is an <b>.stl</b> file. The green bounding box in (c) indicates the domain used for meshing and STL export. . . . .	16
3.3	Post-processing pipeline: (a) original foam reconstruction and mesh, (b) remeshed and simplified geometry. . . . .	17
3.4	Geometrical models employed in this study: structured and unstructured foam domains across different sizes (1D, 2D, 3D, 4D). All geometries were generated via Poisson-based reconstruction and cleaning workflow. . . . .	18
3.5	Single Plateau border. . . . .	19
3.6	Generalized setup of the simulation domain. The conducting block (representing the foam geometry in the liquid phase) is embedded between two parallel copper electrodes, across which a potential difference $\Delta V$ is applied. The surrounding airbox is treated as an insulating domain. . . . .	21
3.7	Simulation setups: (a) unstructured foam geometry, (b) single Plateau border geometry. . . . .	23
3.8	Refined triangular element (h-refinement) drawn in PowerPoint to present the idea of $h$ .Specifying the maximum length of tetrahedra on faces or inside of objects. When the initial mesh has been generated, the refinement of triangle elements as per the $h$ value will refine the initial mesh. . . . .	24
3.9	Mesh convergence study on the single Plateau Border (PB): (a) percent deviation in current, and (b) stabilization of relative conductivity. . . . .	25
3.10	Mesh visualization of foams: (a,b) unstructured foam with full mesh and zoomed region. . . . .	26
3.11	Meshed view of complete simulation domain. . . . .	26
4.1	Voltage distribution across the structured foam simulation. . . . .	28

4.3	Conductivity analysis in unstructured foams: (a) relative conductivity and (b) normalized relative conductivity with error bars. . . . .	30
4.4	Directional relative conductivity $\sigma_{\text{rel}}$ for the structured foam at $\phi = 5.53\%$ , compared against classical models of Feitosa, Lemlich and Maxwell pre- dictions. . . . .	31
4.5	Comparison of structured and unstructured foam conductivities at specific liquid fractions using Feitosa normalization. . . . .	32

# List of Tables

3.1	Mesh convergence study on single Plateau Border (PB) . . . . .	24
3.2	Liquid fraction $\phi_l$ (%) for the unstructured and structured foam by size. . .	27

# Chapter 1

## Introduction

### 1.1 Application and Relevance of Liquid Foams

Foam, a substance that at first glance seems simple, is made from gas dispersed in a liquid or solid and plays a rich and varied role in both nature and human culture. Mythologically, foam appears in tales from the Mahabharata to Greek and Chinese legends, symbolizing transformation, creation, and mystery. In everyday life, its presence is evident in food and drink, from the stable froth of beer and cappuccino to airy mousses and baked goods, where proteins or gelling agents help maintain structure. Often, surfactants (surface-active substances that reduce surface tension and stabilize bubbles) from pollutants or organic matter stabilize naturally occurring foams.

Foams are stabilized by agents that adsorb at gas–liquid interfaces, including surfactants, solid particles, and polymers. Among these, surfactants are the most common in liquid foams. They lower the surface tension to facilitate the formation of bubbles. Once at the interface, they help maintain thin liquid films between bubbles through a balance of repulsive forces (known as disjoining pressure), which prevents the bubbles from merging. Beyond the molecular action of surfactants, the structural properties of a foam are also determined by its liquid fraction. The amount of liquid contained in a foam is defined by the liquid volume fraction [4]:

$$\phi_l = \frac{V_l}{V_{\text{foam}}}, \quad (1.1)$$

where  $V_l$  is the volume of liquid and  $V_{\text{foam}}$  is the total foam volume.

While liquid foams can be classified by their stabilizing agents or applications, they are commonly described by their liquid fraction; therefore, the resultant classification: dry foams and wet foams[9].

They can also be classified based on physical state. Liquid foams could be defined as gas bubbles dispersed in a continuous liquid phase, and solid foams could be described as gas bubbles trapped in a continuous solid matrix[2], [4].

### 1.2 Liquid Foam Structure

A liquid foam is a two-phase system in which gas cells are enclosed by a liquid, with adjacent bubbles separated by thin liquid films known as lamellae. When these films converge, they form thicker liquid channels called *Plateau borders*. At the junctions

where four Plateau borders meet, *nodes* (or vertices) are formed. Foam structures tend to minimize surface energy, and the resulting arrangement of films and borders gives rise to their characteristic cellular architecture[4][2].

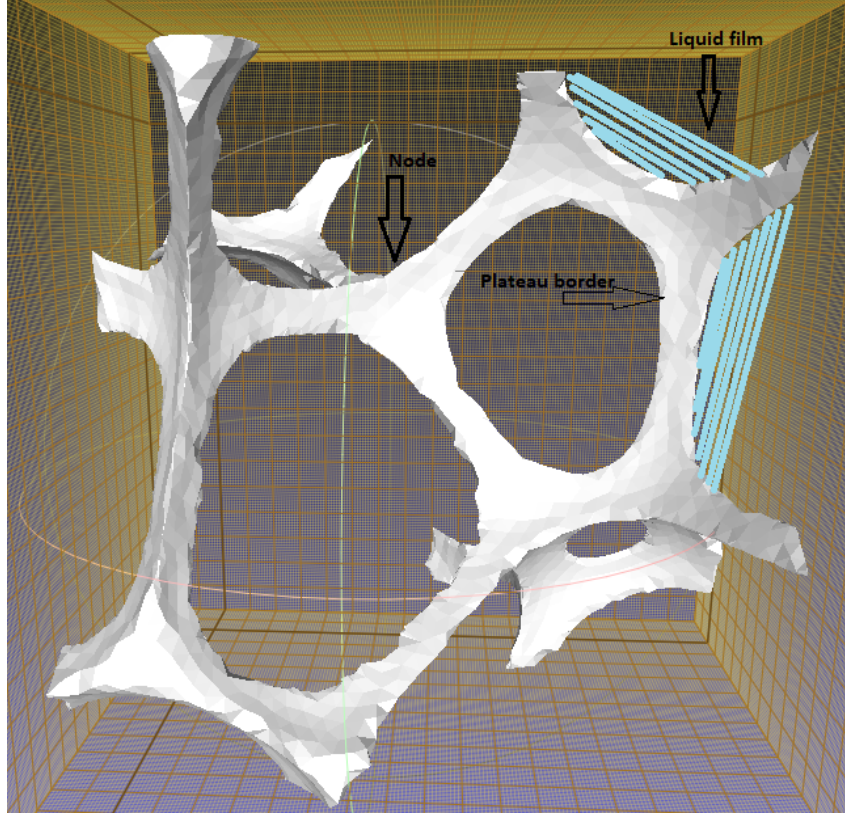


**Figure 1.1:** Three dimensional visualization of the structure of a liquid foam, showing its key elements: **liquid films (lamellae)** separating adjacent bubbles, **Plateau borders** where three films meet, and **nodes (vertices)** where four Plateau borders converge.

## Fundamental Features of Foams

**Liquid Films** Films are thin liquid layers that separate the faces of bubbles. These films can vary in thickness from a few nanometers to micrometers and are stabilized against rupture by surfactants. If the films become too thin, they may rupture, causing the coalescence of bubbles. In wet foams, films are less pronounced, and bubbles remain nearly spherical, whereas in dry foams, these films form the polygonal faces of polyhedral bubbles[4].

**Plateau Borders** When three films meet, they form liquid-filled channels called *Plateau borders*. At the junctions where four Plateau borders converge, *nodes* are formed. The geometry and size of the Plateau borders depend strongly on the liquid fraction of the foam[4].

**Liquid Fraction** The liquid fraction can be defined as the liquid volume fraction given by Eq. (1.1). The liquid fraction helps define different structures depending on a threshold value; the *critical* threshold of liquid fraction, approximately  $\phi_l \approx 0.36$ , corresponds to the random close packing limit of spheres, which indicates that above this value bubbles

are separated, remain spherical, and do not touch each other, making a bubbly liquid. In contrast, below it bubbles are in contact and no longer spherical. [4], [37].

1. Bubbly liquid when  $\phi_l > \phi_l^*$
2. Wet foam for  $0.05 \lesssim \phi_l < \phi_l^*$
3. Dry foam when  $\phi_l \lesssim 0.05$

The lower threshold at  $\phi_l \approx 0.05$  is a conventional value and not a strict geometrical boundary used in foam physics to distinguish wet from dry foams[4].

Classifications of foam structures can be made based on bubble size distribution and spatial arrangement as follows:

- **Bubble size distribution:**
  - **Polydisperse foams:** Bubbles have a wide range of size distribution and typically lead to irregular packing; films and Plateau borders vary in thickness[4].
  - **Monodisperse foams:** Bubbles are more uniform in size, and typically more ordered structures[2]. However, monodispersity does not automatically imply crystallinity; even foams with equal-volume bubbles may remain disordered, as demonstrated in studies of random monodisperse foams[18]
- **Spatial arrangement:**
  - **Structured foams:** Bubbles are arranged in an ordered lattice, often monodisperse[37].
  - **Unstructured foams:** Random bubble arrangement, often polydisperse[37].

### 1.2.1 Important Processes In Liquid Foams

#### Drainage

Drainage is defined as the process by which liquid flows through the foam's network of Plateau borders and nodes, often driven by gravity and capillarity. This phenomenon leads to the drying of the foam over time, resulting in the thinning of the films and an increased susceptibility to rupture. The ability to effectively regulate drainage is crucial for optimizing the longevity and performance of foam in food products, firefighting foams, and industrial applications [4], [27].

#### Coarsening

Coarsening is defined as the growth of larger bubbles at the expense of smaller ones, resulting in alterations to the foam structure and properties over time. This process has a significant impact on the physical characteristics of the foam, including its texture, mechanical stability, and overall lifespan [4], [27].

### Film rupture and coalescence

The phenomenon of foam coalescence is attributed to the rupture of liquid films that separate gas bubbles, resulting in the merging of bubbles and a reduction in foam stability. The stability of the film depends on the concentration of the surfactant and the chemical composition. Management of foam collapse is imperative for two fundamental applications: first, to extend the duration of foam presence in cleaning or food applications; and second, to inhibit foam where its presence is deleterious, such as in chemical reactors [4].

### 1.2.2 Dry and Wet Foams

As discussed in Section 1.1, foams can be further distinguished as dry or wet systems.

In dry foams (typically  $\phi_l < 5\%$ ), the bubbles are tightly packed and separated by thin films. In dry foams, bubbles take the form of a polyhedral shape, and the cross-section of the Plateau borders becomes very small. The structure still follows Plateau laws: three films meet at  $120^\circ$  in a Plateau border, and four Plateau borders converge at a node at the tetrahedral angle of approximately  $109.5^\circ$ [4].

Because the liquid films are very thin, the stabilization of dry foams is governed by *disjoining pressure*, which reflects a balance of forces acting between the two surfactant-coated interfaces of the film. The attraction between interfaces comes mainly from van der Waals forces (weak molecular pull between the interfaces). At the same time, repulsion arises from electrostatic forces (repulsion between charged surfactant layers). When the repulsive forces dominate over the van der Waals attraction, the thin film remains stable, thereby preventing its rupture and the subsequent merging of bubbles [4].

With a rise in liquid content, the foam transitions to a wet regime. In wet foams, Plateau borders become thicker, films shrink or even disappear, and the bubbles take on a more spherical shape. Most of the liquid resides in the borders and vertices rather than in the films. Liquid drains downward due to gravity, establishing a vertical pressure gradient. This process leads to *hydrostatic equilibrium*, in which liquid accumulates at the bottom of the foam; hence, wet foams exhibit a non-uniform liquid fraction along the vertical direction. The corresponding microstructural features can be summarized as: [4].

- Bubbles retain approximately constant gas volume on short timescales; shapes become more spherical as liquid fraction increases.
- Soap films' surface area decreases with liquid fraction, and film thickness remains negligible relative to Plateau border size.
- Plateau borders are formed, which thickens with increasing liquid fraction, and borders may locally merge, changing connectivity of neighboring vertices.

### 1.2.3 Mechanical Properties of Liquid Foams

Essential properties to consider in Liquid foams are viscoelasticity, elasticity, yield stress, energy dissipation, and dependence on liquid fraction.

#### 1. Viscoelastic Nature

Liquid foam can behave like weak viscoelastic solids. For smaller deformations, bubbles distort slightly, while for larger deformations, bubbles exhibit plastic flow, which means they undergo irreversible bubble arrangements.[4].

## 2. Yield Stress and Damping

Foams have a finite yield stress, defined as the stress below which the material deforms elastically; they behave elastically and viscoelastically below the yield stress, and above the yield stress they flow like a viscous liquid—typically shear-thinning (the apparent viscosity decreases as the shear rate increases)—via bubble rearrangements[37]. This rearrangement of bubbles makes them efficient damping materials that can absorb and dissipate mechanical energy [4].

## 3. Effect of Liquid Fraction

Dry foams have high shear modulus (elastic resistance is mainly due to surface tension acting on thin films) and high yield stress behaving more like solid, while wet foams have lower modulus and yield stress [4].

The distribution of liquid fraction also determines the overall behavior of foams, since it is closely related to bubble size: foams with smaller bubbles generally retain more liquid, while larger-bubble foams are typically drier. Thus, foam rheology is strongly dependent on liquid fraction. In addition to mechanical properties, the liquid fraction also governs transport processes in foams, such as electrical and thermal conductivity, and to some extent permeability. A higher liquid fraction facilitates easier fluid and gas transport through Plateau borders and nodes, which tends to affect foam permeability [22], [28], [33].

## 1.3 Electrical Conductivity

The electrical conductivity of a liquid foam is the effective (bulk) conductivity of the two-phase structure, quantifying how easily electric current passes through the foam’s continuous liquid network (Plateau borders and nodes) while the gas phase is essentially insulating. It depends mainly on the liquid fraction  $\phi_l$ , the conductivity of the liquid  $\sigma_{\text{liquid}}$ , and the geometry/topology[4], [35].

Bulk (effective) conductivity is a single macroscopic number that indicates how electricity flows through the entire foam, not just one tiny liquid channel. It differs from the conductivity of liquids, as foam has a gas phase that is non-conducting and a complex network of liquid paths and junctions, which lowers the overall bulk value. The bulk conductivity of any homogeneous bulk sample can also be expressed in terms of its measured electrical resistance  $R$  as

$$\sigma_{\text{eff}} = \frac{L}{RA}, \quad (1.2)$$

where  $L$  is the electrode separation (distance between two electrodes),  $A$  the electrode cross-sectional area, and  $R = V/I$  the measured resistance of the sample [35].

To make results comparable across different liquids, we often report the relative conductivity (bulk conductivity divided by the liquid’s conductivity)[35].

The relative conductivity is defined as

$$\sigma_{\text{rel}} = \frac{\sigma_{\text{foam}}}{\sigma_{\text{liquid}}} = \sigma(\phi_l) \quad (1.3)$$

where  $\sigma_{\text{foam}}$  is the effective bulk conductivity of the foam and  $\sigma_{\text{liquid}}$  is the conductivity of the pure liquid phase and  $\phi_l$  denotes the liquid fraction. Liquid foam conductivity depends on the connectivity of Plateau borders and nodes, as well as the liquid fraction.

The electrical conductivity of foam can be significantly reduced because the fluid pathways in foam are often tortuous and discontinuous compared to those in a pure liquid phase. Some classical models examine the relationship between electrical conductivity and liquid fraction, offering insights that can inform further analysis and comparison. Hence, electrical conductivity offers an indirect but effective approach for studying the liquid fraction of foam[4].

Building on this, since the gas phase is essentially insulating, electrical conduction occurs almost entirely through the interconnected liquid network, making the electrical conductivity of foam significantly dependent on liquid fraction and hence widely used in laboratories and industry as a practical and reliable method to define and monitor the liquid fraction in foams[11], [38].

## Tortuosity

The complexity of transport pathways in foams and other geometries is characterized by a parameter called tortuosity[6]. It is defined as the ratio between the effective path length through the medium and the straight-line distance:

$$\tau_\ell = \frac{L_{\text{eff}}}{L} \geq 1, \quad (1.4)$$

where  $L_{\text{eff}}$  is the effective path length and  $L$  is the straight-line distance[6].

For transport in porous media, it is common to use the tortuosity factor  $\tau_F$  which, in the simplest picture, scales as

$$\tau_F \approx \left( \frac{L_{\text{eff}}}{L} \right)^2, \quad (1.5)$$

possibly augmented by a constriction factor to account for narrow connections between Plateau borders and nodes, which locally increase resistance. Under this convention, the effective electrical conductivity of a liquid-saturated porous network can be expressed as

$$\sigma_{\text{eff}} = \frac{\phi}{\tau_F} \sigma_{\text{bulk}}, \quad (1.6)$$

so that tortuosity (and constrictions) reduce  $\sigma_{\text{eff}}$  below the bulk fluid value.[34]

In foams, the geometry of Plateau borders and solid struts forces the transport of fluids to follow longer trajectories compared to free space, contributing to tortuosity. Tortuosity helps to explain why the effective conductivity of foams is reduced compared to the bulk liquid. If current could flow in straight paths, conductivity would scale linearly with liquid fraction (as in Archie's law for porous media)[3]. Instead, tortuous pathways lower the effective transport[4]. Hence, it could be that electrical conductivity, permeability, and diffusive transport could be directly affected by tortuosity.

## 1.4 Solid and Liquid Foams

Solid and Liquid foams share fundamental cellular architecture; however, their physical properties differ significantly due to the nature of the continuous phase[4], [27].

In liquid foams(e.g., including soap froth and firefighting foams), gas bubbles dispersed in the liquid phase are stabilized by surfactants. Two important aspects of liquid films include the thinning of liquid films due to gravity and capillary forces, which result in

thicker Plateau borders and nodes. Secondly, over time, smaller bubbles shrink and disappear, while larger bubbles grow, leading to coarsening [4].

While in solid foams(examples of solid foams can be polyurethane and polystyrene foams), cells are obtained from the solidification of the liquid phase, the thin films and Plateau borders become rigid cell walls. Furthermore, they can be classified into open-cell (where pores are interconnected) or closed-cell (where pores are isolated). Solid foams exhibit high thermal and acoustic insulation properties [12].

With the solidification process, it is possible to capture the cellular structure of foams using liquid foams as templates[2], [9]. However, the present study focuses on liquid foams. The primary distinction between solid and liquid foams can be stated as follows: liquid foams are transient and evolve, whereas solid foams, once formed, retain their structure [4], [27].

## 1.5 Research Focus

Conventionally, theoretical and experimental studies have centered on two distinct categories of foams: highly idealized (structured) foams, exemplified by monodisperse, ordered lattices, and real, unstructured foams characterized by random bubble sizes and arrangements. Since a material's structure largely determines its macroscopic behaviour, it is reasonable to expect that random and structured foams might exhibit different transport and mechanical responses. In the meticulous optical study of Matzke(1946)[23], it was revealed that random foams contain virtually no Kelvin cells, underlining the rarity of ordered structures in natural foams. (2023)[32] used neutron radiography to show that foam structure near solid walls modifies liquid fraction profiles and reduces permeability. However, the effect of foam structure—i.e., the influence of the ordering of bubbles and the uniformity of liquid channels on overall conductivity—remains to be fully comprehended. Chammouma et al. (2025)[5] demonstrated that guiding bubble self-assembly with fiber arrays enables the formation of long-range ordered Kelvin and HCP foams, and crucially showed that this order is preserved after solidification.

Addressing this gap, the objective of this study is to utilize a simulation approach to compare the electrical conductivity of structured and unstructured foam geometries across different liquid fractions. The aim of these simulations is twofold: first, to quantify the influence of foam structure on conductivity at varying liquid fractions. Additionally, the study aims to assess the reliability of conductivity measurements as an indirect method for evaluating foam structure or liquid content in experimental systems. By establishing a connection between the idealized models and the actual foam structures, this research contributes to a deeper understanding of the interplay between foam geometry and electrical conductivity.

# Chapter 2

## Theoretical Background and State of the Art

### 2.1 Overview of Foam Structure and Transport Properties

Building on the framework established in Chapter 1, highlights that the foam microstructure—comprising thin films, Plateau borders, and vertices—forms a tortuous liquid network that governs transport phenomena. Electrical conductivity is particularly powerful in this context: beyond being a fundamental physical quantity, it is widely used across both industrial and laboratory settings as a diagnostic measure, and is intimately linked with thermal transport, acoustic attenuation, permeability, and mechanical stability[4], [11], [19]. Lamolinairie *et al.*(2022)[19] demonstrated how electrical conductivity can be combined with neutron scattering and imaging to probe foam structure across multiple length scales, revealing its connection to liquid fraction and structural metrics. In the present work, tomography data from Chammouma et al. [5] provided data on the structured and unstructured liquid foam geometries. Since experimental studies cannot easily isolate the separate influences of foam structure and liquid fraction, numerical simulations offer a complementary solution, allowing for a controlled comparison between structured and random foams. Numerical simulations have long been employed to probe how foam morphology, porosity, and tortuosity influence transport properties in a controlled, systematic manner—capabilities that are often beyond the reach of traditional experimental setups[10], [20]. In the present study, simulations applied to tomography-based geometries enable the investigation of the relationship between foam geometry and electrical conductivity without relying solely on idealized models.

### 2.2 Electrical Conductivity of Liquid Foams

Electrical Conductivity is closely associated with the liquid volume fraction, the three-dimensional connectivity of the liquid pathways, and the geometric configuration of the foam. The relation taken from equation (1.3) provides a theoretical basis for modeling foam transport and a practical tool for interpreting experimental data. The study of foam conductivity is based on essential theories like percolation theory and network analysis, as well as analogies to transport in porous materials[20], [30]. This area of research is important because it links fundamental science with real-world engineering applications.

In liquid foams, the gas phase is effectively non-conductive because gases have extremely low electrical conductivity. Primarily, due to the very low density of free charge carriers, electric current cannot pass through the gas bubbles and conduction is possible only through the interconnected liquid network [37].

Contributions from thin liquid films in modeling the electrical conductivity of liquid foams can be approximated as additive, weighted by their liquid volume fractions:

$$\sigma = \sigma_{\text{pb}} \phi_{\text{pb}} + \sigma_{\text{film}} \phi_{\text{film}}, \quad (2.1)$$

where  $\phi_{\text{pb}}$  and  $\phi_{\text{film}}$  denote the fractions of the total liquid fractions in Plateau borders and films, respectively [37]. The total liquid fraction is given by [37]

$$\phi_l = \phi_{\text{pb}} + \phi_{\text{film}}. \quad (2.2)$$

Although conductivity may increase slightly with the total liquid fraction due to film thickening under pressure, no regime has been identified in which the film contribution dominates. In fact, the relative contribution of films tends to vanish in the dry limit ( $\phi_{\text{film}} \rightarrow 0$ ), so electrical conduction is effectively governed by the Plateau border network[4].

The electrical conductivity of liquid foams is complex and has been extensively modeled. Various classical models relate effective conductivity to liquid fraction, serving as benchmarks for experimental and numerical studies. Lemlich model describes the dry-foam limit, while the Maxwell model applies in the dilute suspension limit. These classical models have been connected by the empirical relation proposed by Feitosa *et al.*, which interpolates between the asymptotic behaviors of Lemlich and Maxwell, yielding a consistent description of conductivity across the full range of liquid fractions[8], [11], [24].

### 2.2.1 Lemlich Model

The description of the effective electrical conductivity of liquid foams in the dry regime was proposed by Lemlich [8]. The basis of the model considers a polyhedral foam structure where the liquid fraction is sufficiently low such that all of the conductive liquid is confined to the Plateau borders, and the contribution from thin films can be neglected. The foam is treated as a random lattice of narrow, electrically conductive channels, the Plateau borders, embedded in a nonconductive gas matrix.

Assuming a random distribution of border orientations in a three-dimensional (3D) isotropic foam, Lemlich[8] derived a relationship between the conductivity ratio

$$\sigma_{\text{rel}} = \frac{\sigma_{\text{foam}}}{\sigma_{\text{liquid}}} = \frac{1}{3} \phi_l$$

and the liquid fraction  $\phi_l$ . Here,  $\sigma_{\text{foam}}$  is the effective conductivity of the foam and  $\sigma_{\text{liquid}}$  is the conductivity of the continuous liquid phase. This equation indicates that electrical conductivity is directly linked to the amount of liquid available in the foam and the structural connectivity provided by the Plateau borders. The factor  $\frac{1}{3}$  emerges from averaging the directional components of current through a randomly oriented network of one-dimensional conductive elements in three-dimensional space.

This model establishes a linear dependence of conductivity on liquid fraction, providing a baseline for experimental and numerical studies in the dry limit. Notwithstanding these constraints, the Lemlich model remains a fundamental reference in the foam conductivity literature and will be utilized in this study as a benchmark for comparing simulation outcomes within the dry regime.

## 2.2.2 Maxwell model

The Maxwell model[24], originally developed for heterogeneous media containing spherical inclusions, represents one of the most influential theoretical approaches for predicting the effective conductivity of dispersed systems. Upon applying the model to liquid foams, it considers the foam as a continuous liquid matrix containing dispersed, non-conducting gas bubbles. The framework relates the bulk foam conductivity to its liquid fraction.

The classical Maxwell equation for electrical conductivity in foam systems is expressed as:

$$\sigma_{\text{rel}} = \frac{\sigma_{\text{foam}}}{\sigma_{\text{liquid}}} = \frac{2\phi_l}{3 - \phi_l} \quad (2.3)$$

This expression is obtained by solving Laplace's equation for the electrical potential in a medium comprising randomly distributed spherical inclusions, with appropriate boundary conditions[24].

The Maxwell model is predicated on several key assumptions that define its domain of applicability. Firstly, it is assumed that the dispersed phase (gas bubbles) is perfectly non-conducting. Secondly, the model operates under the assumption that the bubbles retain a spherical geometric form.

## 2.2.3 Empirical relation of Feitosa *et al.*

Feitosa *et al.* proposed a relation between the relative conductivity as a function of liquid volume fraction for the entire range of dry foams to wet suspensions; the model fits well with the limitations proposed by Lemlich and Maxwell as well. The assumptions for the model are an isotropic, well connected liquid network.

Following Feitosa *et al.* [11], the relative conductivity  $\sigma_{\text{rel}}$  and the liquid fraction  $\phi_l$  are taken as the key variables (see Eq. ??). They proposed rational functions that (i) match the Maxwell and Lemlich limits and (ii) fit experimental conductivity data reported in their study covering from dry foams to wet suspensions[11]:

$$\sigma_{\text{rel}}(\phi_l) = \frac{2\phi_l(1 + 12\phi_l)}{6 + 29\phi_l - 9\phi_l^2}, \quad (2.6)$$

$$\phi_l(\sigma_{\text{rel}}) = \frac{3\sigma_{\text{rel}}(1 + 11\sigma_{\text{rel}})}{1 + 25\sigma_{\text{rel}} + 10\sigma_{\text{rel}}^2}. \quad (2.7)$$

These recover the accepted limits: Maxwell's wet limit  $\sigma_{\text{rel}} \rightarrow 2\phi_l/(3 - \phi_l)$  as  $\phi_l \rightarrow 1$  and Lemlich's dry limit  $\sigma_{\text{rel}} \sim \phi_l/3$  as  $\phi_l \rightarrow 0$ . Near the wet limit,  $\sigma_{\text{rel}} = 1 - \frac{3}{2}(1 - \phi_l) + (0.65 \pm 0.01)(1 - \phi_l)^2 + \mathcal{O}((1 - \phi_l)^3)$ ; near the dry limit,  $\sigma_{\text{rel}} = \phi_l/3 + (2.0 \pm 0.4)\phi_l^2 + \mathcal{O}(\phi_l^3)$  [11]. Using (2.6) to predict  $\sigma_{\text{rel}}$  from a known  $\phi_l$  and (2.7) to estimate  $\phi_l$  from measured  $\sigma_{\text{rel}}$ .

## 2.3 Role of Microstructure

### 2.3.1 Structured Foams

Structured foams as defined in section 1.2 are characterized by bubbles arranged in an ordered lattice. Research emphasizes advanced approaches; the creation of monodisperse, periodic structures with uniform bubble geometry is possible through advanced

approaches such as microcellular foaming, templating, and gas-assisted expansion, making it possible to have careful control over bubble nucleation and growth, enabling narrow size distributions and ordered structures[2], [26].

Preserving ordered architecture over time is a critical challenge. Solidification or freezing of liquid foams is possible through processes such as polymerization, curing, or crosslinking [16]. Additionally, on a similar note, Antje Van der Net *et al.* (2009)[26] found that the ordered regions, where bubbles were arranged neatly, only extended over a limited area and became irregular globally, which limits the possibility of producing large samples with perfect long-range order. The study also demonstrated that anisotropy and connectivity can be deliberately tailored, thereby opening up opportunities for directional applications.

Nevertheless, a study done by Antje Van der Net *et al.* (2009)[26] identified that such structured materials have promising applications in catalysis, for separation membranes, and filtration.

In addition to experimentally fabricated structured foams, widely studied geometric models of dry foam include the Kelvin and Weaire–Phelan structures[4]. The Kelvin structure proposes partitioning space into identical truncated octahedra of equal volume, each with a minimal surface area[4], [37]. An alternative to this was the Weaire–Phelan structure, which advanced Kelvin’s findings by integrating two distinct cell types, thereby achieving a further reduction in the total area. Both structures follow the Plateau laws. Consequently, they are regarded as physical examples of dry foams[4].

### Kelvin Cell: An Ordered Foam Model

Kelvin cell for foams is important ordered reference structure, which represents unit cell of an ordered monodisperse foam with liquid fraction less than 6.3 percent[4]. It has body centred cubic arrangement of bubbles, where each bubble shares six square faces and eight hexagonal faces with its neighbors. Edges thicken into Plateau borders when finite liquid fraction is introduced, where  $r_{PB}$  is radius of Plateau border[4].

The volume contributions to the total liquid fraction  $\phi_l$  go as follows:

- Volume of Plateau borders scale quadratically with Plateau border radius:

$$V_{PB} \propto r_{PB}^2,$$

- Vertices scale cubically:

$$V_n \propto r_{PB}^3,$$

- Films contribution is negligible[4], [37].

Thus, the liquid fraction  $\phi_l$  of a Kelvin cell can be approximated as[4]:

$$\phi_l \approx 0.171 \left( \frac{r_{PB}}{R_V} \right)^2 + 0.200 \left( \frac{r_{PB}}{R_V} \right)^3, \quad (2.4)$$

where  $R_V$  denotes the radius of a sphere having the same volume as the Kelvin bubble (i.e., the unit cell of the ordered foam)[4].

For very small liquid fractions ( $\phi_l < 1\%$ ), the cubic term can be neglected, giving[4].:

$$\phi_l \approx 0.33 \left( \frac{r_{PB}}{R_V} \right)^2. \quad (2.5)$$

### Foams with translational symmetry

When the pore or bubble arrangement is not purely random but is intentionally controlled during fabrication, for example, by using techniques like templating, or 3D printed matrices which guide bubble size and connectivity during foaming, are helped to achieve partial ordering in structured foams[2].

A particular case is that of patterned foams with translational symmetry in which bubble and their Plateau borders are organized into parallel planes, giving a foam a distinct translational order in one direction. It has been experimentally seen by Albuquerque and Fortes [1] that such layering can be introduced mechanically by traversing pins through bamboo foams, where snapping and reconnection of films causes Plateau borders to reorganize. Such approaches demonstrate that order can be mechanically induced in initially random foams; however, these results are more precise in quasi-2D systems and do not extend to typical three-dimensional liquid foams, while dynamic structure—subject to drainage, coarsening, and film rearrangements—rapidly erases any mechanical patterning, making sustained order practically unattainable in typical 3D liquid foams[13].

## 2.4 Existing Models, Simulation Approaches, and Motivation

Models for foam conductivity have traditionally focused on limiting cases. Current models and studies emphasize either the dry regime, where conduction is dominated by Plateau borders and films, or the wet regime, where bubbles behave as insulating inclusions in a continuous liquid phase. Lemlich's law [21] and Maxwell's equation [24] set reliable limits on these extremes. However, Feitosa [11] measured conductivity of 3D foams across a wide range of liquid fractions and proposed a model that fits between extreme limits. Yazhgur *et al.* [38] showed the role of surface Plateau borders and nodes is significant in quasi-2D foams, stating that models for extreme limits miss the significant role of Plateau borders in the intermediate region.

Few recent studies have depicted how different modeling strategies can be used to link foam geometry to macroscopic properties. In a study conducted by Jung [17] on an open-cell aluminium alloy foam, geometry was determined using a fold approach and binarized micro-tomography images, which were then used for direct FEM simulations. Moreover, the second method involves fitting a random Laguerre tessellation to the same micro tomography dataset to generate another sample for foam geometry. FEM simulations are then performed on this sample, and the output measures the effective elastic modulus. Another study of heat transport in liquid foams, Mobarak [25] chose to represent foam geometry using a computational lattice (a regular grid lattice, essentially a 3D grid), where certain regions of the lattice were designated as liquid channels and the rest as gas, to mimic foam geometry. Using the Lattice Boltzmann Method, simulations were conducted to compute the effective thermal conductivity as a function of liquid fraction.

The present study utilizes tomography-based reconstructions of foam samples [5] to obtain the actual three-dimensional geometry of both structured and unstructured foams, building on the approaches mentioned earlier. Tomography-based geometries preserve natural irregularity while also enabling comparison between structured and random foam. Numerical simulations were performed to compute the relative conductivity of foams as a function of liquid fraction; this choice parallels the thermal conductivity studied by

Mobarak [25] and elasticity by Jung [17], but provides a focus on electrical transport mechanisms, where conduction occurs predominantly in Plateau borders.

# Chapter 3

## Materials and Methods

This chapter focuses on the numerical setup adopted for this research project. Focusing on geometry acquisition, model simplifications, meshing, governing equations, and solver setup.

The flowchart below shows the tool chain used to prepare the foam geometries in the present study. Two types of geometries were considered in this work: (i) a simplified single Plateau border (PB), and (ii) the complete liquid foam geometries. The general tool chain for processing both geometries is illustrated in Fig. 3.1.



**Figure 3.1:** Tool chain used for geometry preparation, generated using the Microsoft PowerPoint presentation tool. The same workflow was applied to both the single Plateau border and the full foam geometry.

### 3.1 Geometry Acquisition and Preparation

Liquid foam geometries used in the present study are constructed from slice images obtained from the experimental research of Chammouma et al. [5], who investigated a novel strategy to induce crystalline ordering in foams (alginate and polyurethane) by guiding the self-assembly of monodisperse bubbles within fiber arrays. The resulting solidified architecture was characterized by sampling grayscale images using X-ray tomography to obtain a complete 3D voxel description of the foam. The raw output of X-ray tomography consists of 3D grayscale voxel data, where intensity values span a continuous range corresponding to air, liquid films, and Plateau borders, fiber, and reconstruction artifacts.

Each scan produced a 3D data set with a spatial resolution of  $25 \mu\text{m}$  voxel size. The bubble diameter,  $D$ , extracted from the scan was 4 mm. The CT scan size for the alginate foam was  $50 \times 50 \times 80$  mm for both with and without fibers (i.e., structured and random foam, respectively) [5]. For structural analysis, a clear distinction between phases is necessary. For this reason, cleaning the image and creating a binary mask are essential steps.

## Segmentation and cleaning of Tomography slices

The goal is to convert CT slices into a binary mask. The MATLAB script used for segmentation and binarisation was provided by Dr.-Ing. Artem Skrypnik and taken for this work. The MATLAB code was generated with the following pipeline of operations

### 1. ROI cropping

ROI cropping reduces computational cost by retaining only the region of interest, defined at a specific position, while discarding the rest of the volume. *Spatial Calibration*

$$M = \frac{1}{25 \times 10^{-3}} \quad [\text{px/mm}], \quad (3.1)$$

$$L_{\text{size,mm}} = 4D \times 4D \quad [\text{mm}], \quad (3.2)$$

$$L_{\text{size,px}} = M L_{\text{size,mm}} \quad [\text{px}]. \quad (3.3)$$

$M$	Magnification factor (px/mm)
<b>where:</b> $p$	pixel pitch (mm/px), with $M = 1/p$
$L_{\text{size,mm}}$	physical length (mm)
$L_{\text{size,px}}$	image length in pixels (px)

### 2. Outlier Denoising

To remove salt-and-pepper noise, preserves edges while removing isolated spikes.

### 3. Intensity Normalization

The cropped image was contrast enhanced by linearly stretching its intensity values to nearly the full 16-bit range to improve the separability of phases.

### 4. Light Sharpening

For sharper edges and a more stable threshold

### 5. Global Otsu Thresholding

Actual Mask creation, which outputs a binary image, 0 for air, 1 for Plateau border.

### 6. Morphological Cleanup

Bridges narrow holes and suppresses isolated noise.

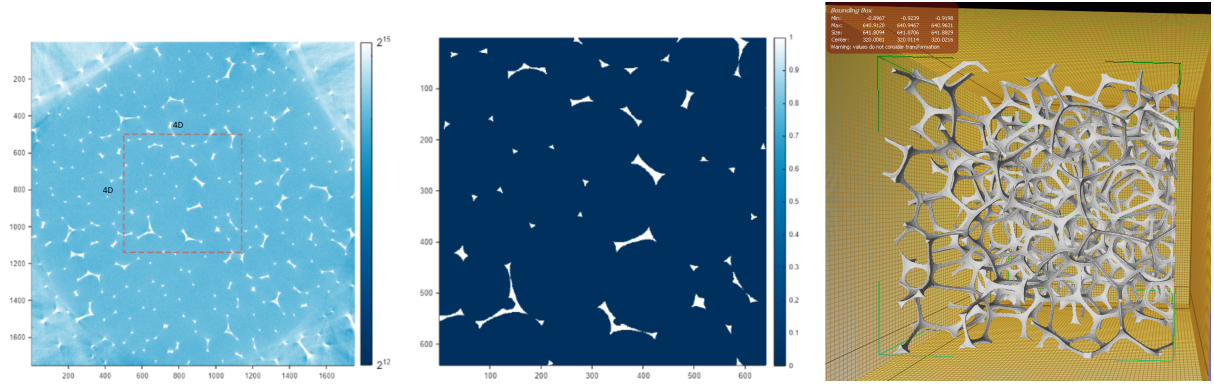
## 3D Slicer

- **Reconstruction in 3D Slicer:**

The binary mask slices are reconstructed into the whole liquid foam geometry using *3D Slicer*. It is a free, open-source software for visualization, processing, segmentation, registration, and analysis of medical, biomedical, and other 3D images and meshes.

- **Stacking and Export:**

After multiple binary masks are generated, they are imported into 3D Slicer. For example, in the 4D dataset, 641 slices were stacked to create a full volumetric mesh from the binary images. The output of Slicer is an **.stl** (stereolithography) file.



(a) Raw CT tomography slice (data courtesy of Marwan Cham-mouma).

(b) Binary mask after segmen-tation.

(c) Volumetric foam structure re-constructed in Slicer.

**Figure 3.2:** Workflow of geometry preparation from tomography data: (a) raw grayscale CT slice, (b) After cleaning and Otsu thresholding (4D x 4D size depicted by red dashed box on raw CT image), a binary mask is obtained (0 = air, 1 = material), suitable for 3D reconstruction.(c) Volumetric unstructured liquid foam reconstruction generated by stacking 641 binary slices.The green box at corners highlights the bounding box for mesh and output is an .stl file. The green bounding box in (c) indicates the domain used for meshing and STL export.

## MeshLab

- MeshLab is an open-source tool for processing and editing 3D triangular meshes. It provides tools for editing, cleaning, healing, inspecting, rendering, texturing, and converting meshes. The four main tasks performed in MeshLab were:
  - **Mesh repair and cleaning:** removing non-manifold faces and unreferenced vertices.
  - **Poisson Surface Reconstruction:** builds a watertight surface from a point cloud by solving a Poisson equation for the indicator function.
  - **Isotropic Remeshing:** improves surface mesh element quality by enforcing nearly uniform edge lengths and reducing skewness.
  - **Calculating Geometrical and topological measures:** MeshLab was used to compute key measures of the reconstructed foam. Below is the formula used to calculate the liquid fraction in the present study

$$\phi_l = \frac{V_{\text{foam}}}{V_{\text{Bounding Box}}} \quad (3.5)$$

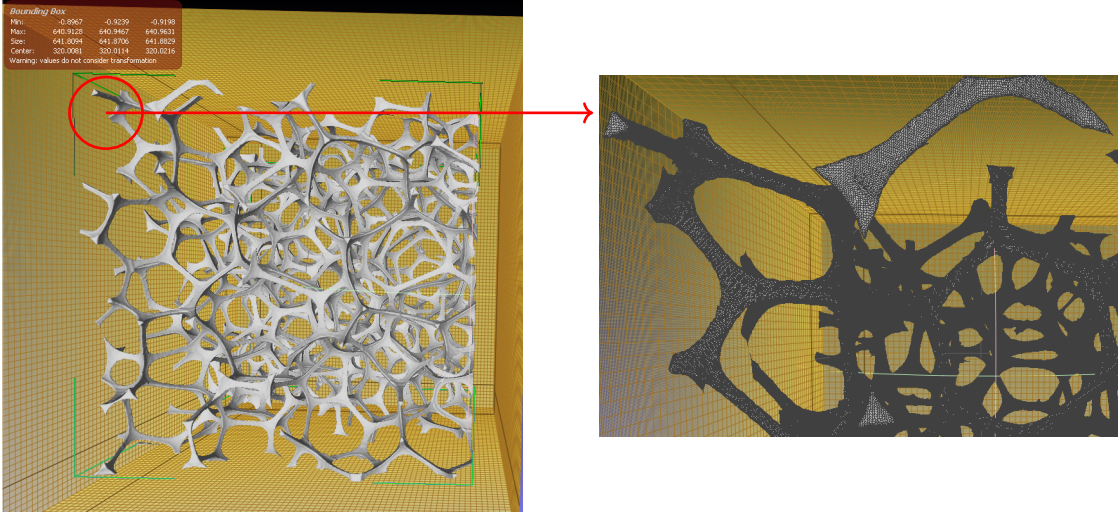
where  $V_{\text{foam}}$  is the foam geometry volume and  $V_{\text{Bounding Box}}$  is the bounding-box volume.

It is important to note that STL files are inherently unitless, and the geometric measures computed in MeshLab are therefore reported in the native units of the mesh.

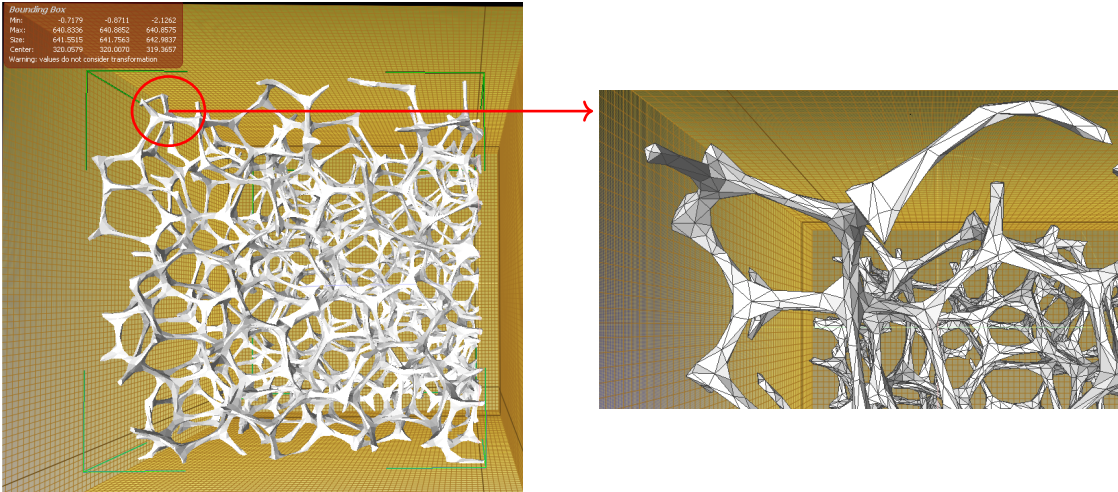
## MeshMixer

Another tool in the workflow was MeshMixer (Autodesk), a free mesh processing and prototyping tool. Further following actions were taken in MeshMixer:

- **Analysis and Repair:** used to repair any non-manifold faces missed by MeshLab.
- **Reduce:** reduces geometry size and file size while retaining the essential geometry.
- **Solidify:** converts surface meshes into solid bodies for further processing.



(a) Foam geometry reconstructed in 3D Slicer from stacked binary masks. The zoomed-in part shows the mesh for the original foam geometry. The original mesh has 7.48M triangular surface elements.



(b) Watertight and remeshed geometry obtained via MeshLab (Poisson surface reconstruction and isotropic remeshing), then simplified in MeshMixer. The zoomed-in part shows the mesh after processing in MeshMixer and MeshLab. The mesh consists of 35K triangular surface elements.

**Figure 3.3:** Post-processing pipeline: (a) original foam reconstruction and mesh, (b) remeshed and simplified geometry.

The geometries used in this study were generated from the workflow mentioned above. For the present study, a series of geometrical models of increasing size was employed, distributed across the following sizes: 1D, 2D, 3D, and 4D. In this classification system, D denotes the diameter of the bubble, which is set at 4 mm. This provides a systematic way to study the influence of volume size on effective conductivity. In addition to these

unstructured cases, a structured benchmark geometry was used for direct comparison in terms of size of 4D.

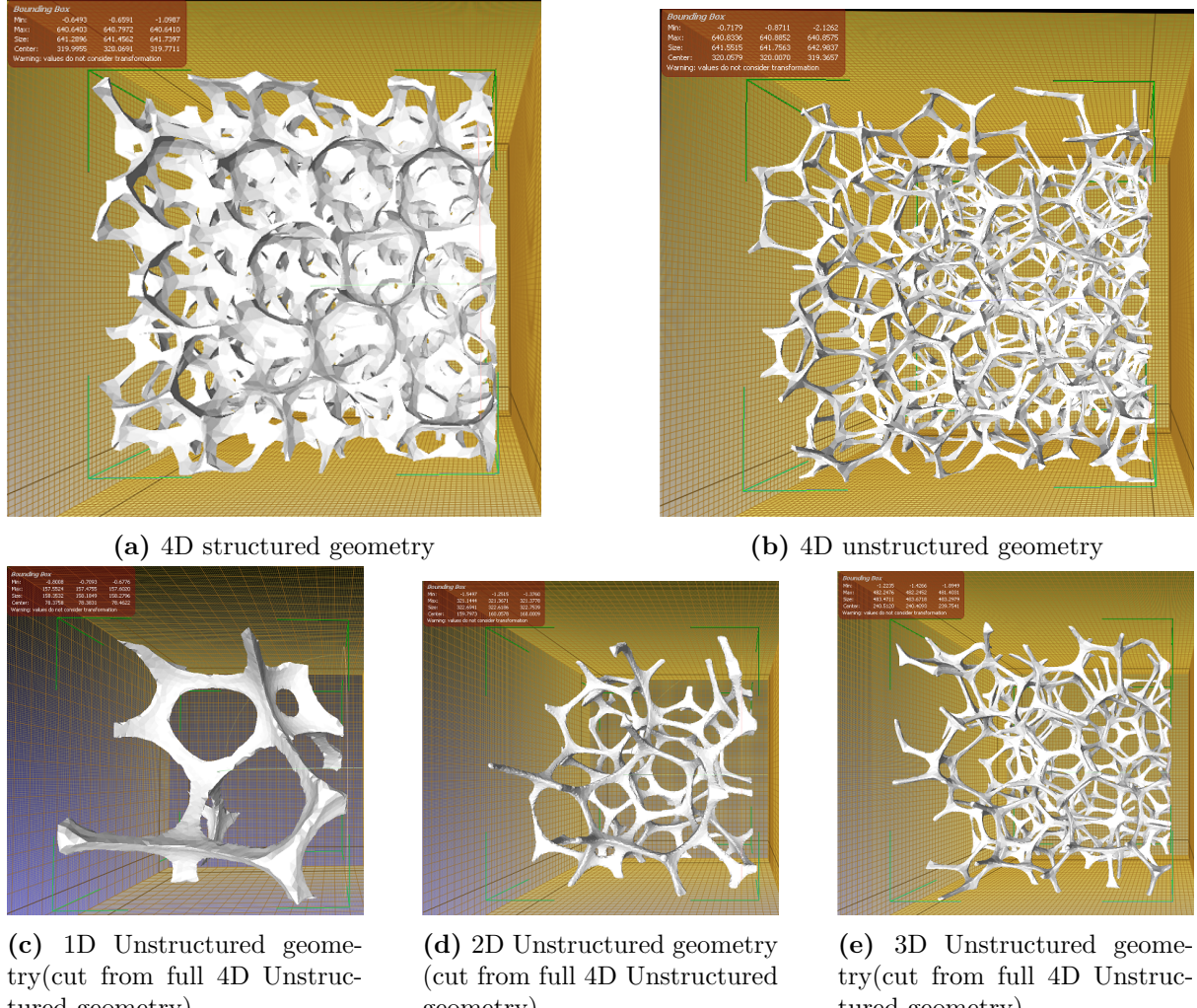


**Figure 3.4:** Geometrical models employed in this study: structured and unstructured foam domains across different sizes (1D, 2D, 3D, 4D). All geometries were generated via Poisson-based reconstruction and cleaning workflow.

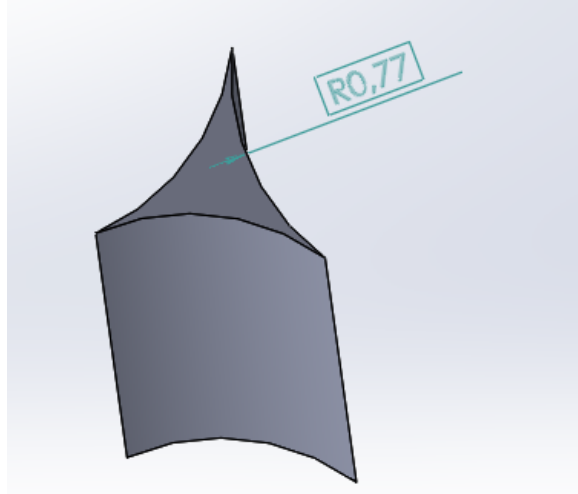
## SolidWorks

SolidWorks is a CAD program for creating parametric models. Assemblies and drawings. The final step in geometry preparation was performed in SolidWorks. In the present workflow, SolidWorks served two purposes:

- **Final processing of foam geometries:** The foam geometries were imported into SolidWorks for solidification and conversion into .STEP files.
- **Creation of simplified single Plateau border (PB) geometry:** The present case is used as a reference for testing boundary conditions and meshing strategies. In accordance with equation (2.7):

$$\phi_l \approx 0.33 \left( \frac{r_{PB}}{R_V} \right)^2, \quad (3.4)$$

which relates the liquid fraction to  $r_{PB}$  (the radius of the Plateau border) and  $R_V$  (the diameter of the bubble, here  $R_V = 2$  mm). Hence, a Plateau border of radius 0.77 mm was generated in SolidWorks and exported as an .STL file. This STL mesh was remeshed in MeshLab to improve element quality and then re-imported into SolidWorks for conversion into a .STEP file.



(a) Plateau border drawn and extruded in SolidWorks.

**Figure 3.5:** Single Plateau border.

## 3.2 Numerical Framework

This section introduces governing equations, assumptions, boundary conditions and global solver setup.

### 3.2.1 Universal Equations, Governing Equation and Assumptions

Partial differential equations (PDEs) are used for modeling electric currents. Electric currents include direct currents (DC), alternating currents (AC) or general time-dependent currents.

The main equation used is the continuity equation for electric current(also known as charge continuity equation), which expresses local charge conservation, meaning the net outflow of current density ( $\nabla \cdot \mathbf{J}$ ) from a small region must equal the rate of decrease of charge density  $\left(\frac{\partial \rho}{\partial t}\right)$  inside that region is given by[29]:

$$\nabla \cdot \mathbf{J} + \frac{\partial \rho}{\partial t} = 0, \quad (3.5)$$

where  $\mathbf{J}$  [A/m<sup>2</sup>] is the electric current density,  $\rho$  [C/m<sup>3</sup>] is the volume charge density, and  $t$  [s] is the time variable.

Equation (3.1) is a direct consequence of charge conservation, obtained by combining Gauss's law for the electric field with the differential form of current continuity [14], [31].

Under the electroquasistatic approximation

$$\frac{\omega\epsilon}{\sigma} \ll 1,$$

displacement currents are negligible compared to conduction currents, making this formulation appropriate for liquid foams. ( $\sigma \sim 1\text{--}5 \text{ S/m}$ ).

This equation does not consider inductive or magnetic effects. In other words, this formulation cannot be used to model inductive or magnetic phenomena. The current continuity equation is typically used to model conductors for which Ohm's law applies. It is not suitable for modeling perfect insulators where the electrical conductivity is zero.

Electric currents can be modeled in two ways:

- **Steady-state simulation**
- **Dynamic simulation**

Both approaches solve a current continuity problem for the scalar electric potential  $V$ . In a steady-state analysis, a direct current flow is generated by a difference in the electric potential. This analysis type is based on the electrical conductivity  $\sigma$  of the material under consideration.

## Governing Equation

**Electroquasistatic assumption.** At low frequencies or for materials with large skin depth, inductive and magnetic effects can be neglected. Under this electroquasistatic approximation, the electric field can be expressed as the gradient of a scalar potential[29]:

$$\mathbf{E} = -\nabla\phi. \quad (3.6)$$

**Steady-state limit.** For direct current (DC) conduction, the steady-state assumption implies  $\partial\rho/\partial t = 0$ . In the absence of time-varying fields, the charge continuity equation reduces to[29]:

$$\nabla \cdot \mathbf{J} = 0. \quad (3.7)$$

**Constitutive relation.** Using Ohm's law, the conduction current density is related to the electric field as[29]:

$$\mathbf{J} = \sigma\mathbf{E} = -\sigma\nabla\phi, \quad (3.8)$$

where  $\sigma$  is the electrical conductivity of the medium. Substituting into the continuity equation gives[29]:

$$\nabla \cdot (\sigma\nabla\phi) = 0, \quad (3.9)$$

which is the governing PDE for steady-state electrical conduction in heterogeneous media (liquid–gas foam).

## General Modeling Assumptions

In applying governing conduction equation to liquid foams, the following assumptions were made[29]:

1. The foam structure is static (no drainage or coarsening).
2. The air (gas) phase is treated as a perfect insulator.

3. The liquid is homogeneous and isotropic with constant conductivity  $\sigma_\ell$ .
4. Electrodes are perfectly conducting and connected to foam.
5. Capacitive and magnetic effects are neglected (electroquasistatic approximation).

### 3.2.2 ANSYS-Based FEM Framework

ANSYS is an interactive software package that uses the FEM analysis to simulate and solve 3D electromagnetic field problems.

The Finite Element Method (FEM) is a numerical technique used to perform finite element analysis (FEA) of any given physical phenomenon. It serves as the basis for many types of simulation software. FEM helps obtain approximate solutions to problems governed by partial differential equations. In the present case, the steady state equation defined in Eq. (3.9) at constant values of electrical conductivity  $\sigma$  is the Laplace equation, which is a special case of elliptical equations[36].

The ANSYS module used in the present study is the ANSYS Maxwell 3D module. In Maxwell 3D environment, the solver could be set to support Electric (Electrostatic, Electric, DC conduction, or a combination of the two with conduction), Magnetostatic, Harmonic, Transient Electric, and other fields. In the present case, the DC conduction solver was employed, which directly solves the steady state equation defined in Eq. (3.9).

#### General Global Simulation Setup:

This subsection describes the general setup for the simulation used in this study for all geometries.

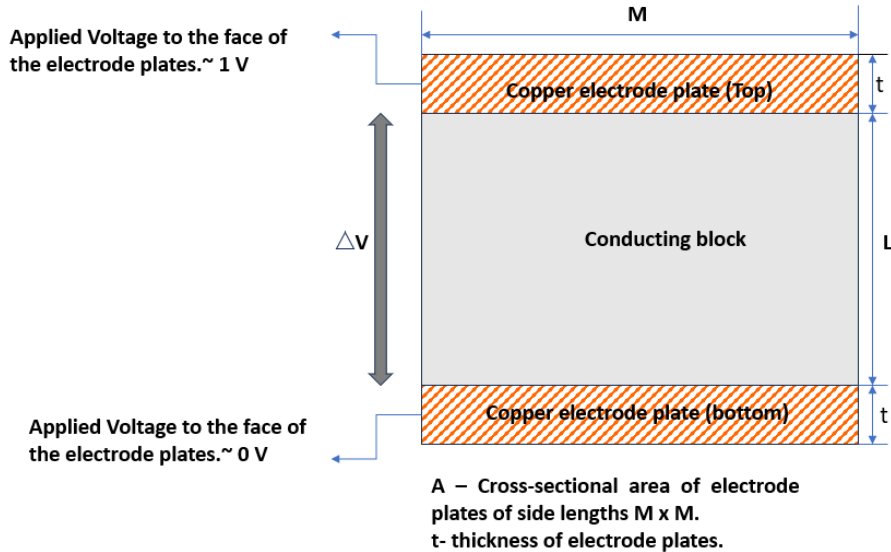


**Figure 3.6:** Generalized setup of the simulation domain. The conducting block (representing the foam geometry in the liquid phase) is embedded between two parallel copper electrodes, across which a potential difference  $\Delta V$  is applied. The surrounding airbox is treated as an insulating domain.

The above figure illustrates the global setup for the simulation domain in 2 dimensions, representing a 3-dimensional setup. The conducting block represents the sample under

study (e.g., foam geometry or any other material with finite electrical conductivity) and is placed between two copper plates, which act as electrodes. All dimensions are considered in SI metric unit.

## Defining Material Domains

The material domains were defined in the DC conduction simulations as follows:

- **Air phase:** FEM requires a closed computational domain; the surrounding air domain gives realistic insulating environment. The surrounding airbox acted as a bounding domain, assigned a electrical conductivity of 0 S/m (perfect insulator).
- **Liquid phase** The liquid foam geometry was modeled using water, with electrical conductivity of 4 S/m.
- **Electrodes:** Two copper plates were placed at opposite ends of the airbox and assigned a bulk conductivity of  $5.8 \times 10^7$  S/m.

## Excitation

Excitation is a source of input

- Applied voltages on faces of the electrodes (Dirichlet values).

## Boundary conditions

To close the problem, appropriate boundary conditions are applied:

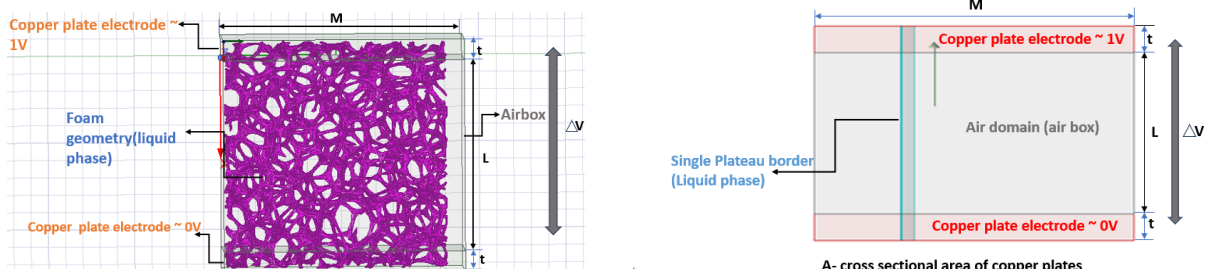
- **Dirichlet (essential):** A fixed potential difference  $V = \bar{V}$  was applied across opposite faces.
- **Neumann (natural):** On all other faces, no boundary condition was explicitly imposed. By default, this corresponds to a homogeneous Neumann condition ( $\mathbf{n} \cdot \mathbf{D} = 0$ ), i.e. no normal flux crossing the boundary.

## Quantities of Interest

The quantities of interest are the current  $I$  obtained after simulation, the effective conductivity  $\sigma_{\text{eff}}$ , and the relative conductivity  $\sigma_{\text{rel}}$ , calculated by adapting Eq. (1.2) and Eq. (1.3), respectively, to specific liquid foam geometries.

## Simulation Setups

Below are the representative setups adapted from the general global setup mentioned in the above sections, used for the geometries chosen in the present case, and will be universal for all other geometries simulated in the present study.



(a) Simulation setup for unstructured foam geometry.

(b) Simulation setup for single Plateau border geometry.

**Figure 3.7:** Simulation setups: (a) unstructured foam geometry, (b) single Plateau border geometry.

Quantities of interest are mentioned in Section 3.2.2. The effective conductivity is obtained from the standard relation taken from equation (1.2) and adapted here for calculation purposes for all geometries. The effective conductivity was calculated as

$$\sigma_{\text{eff}} = \frac{I L}{A \Delta V}, \quad (3.4)$$

where

- $I$  is the conduction current,
- $A$  is the cross-sectional area of the electrode plate,
- $L$  is the distance between the two electrode plates,
- $\Delta V$  is the voltage difference applied across the electrodes.

All dimensions are considered in SI mm units.

For the setup of a single Plateau border, additional quantities are defined as follows:

- **Area (Analytical)**,  $A_{\text{Analyt.}}$ : Measured using the SolidWorks (single Plateau border geometry generated in SolidWorks).
- **Area (Integral)**,  $A_{\text{int.}}$ : Cross-sectional area of the Plateau border calculated after simulation.
- **ANSYS Current**,  $I$ : Current value obtained directly from the simulation in ANSYS.
- **Analytical Current  $I$** : Current value calculated from the geometry using analytical formulae.

### 3.3 Mesh Convergence Study

This section explains one of the many possible meshing strategies chosen for the present study.

### 3.3.1 Mesh Convergence Study on Single Plateau Border

The goal of this analysis was to determine the minimum number of elements that yield accurate results while ensuring that the computed conductivity is mesh independent. The geometry selected here is based on the method explained in Section 3.1.

The maximum target element length in the ANSYS solver is denoted by  $h$ , while  $r_{PB}$  represents the radius of the Plateau border. The *Number of Elements*  $N$  is defined as

$$N = \frac{1}{h/r_{PB}} = \frac{r_{PB}}{h}, \quad (3.10)$$

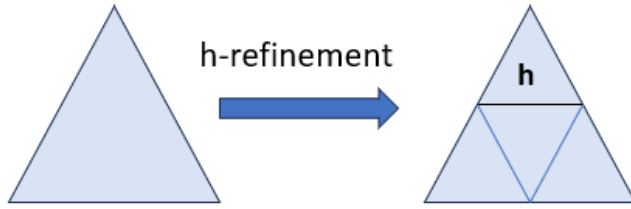
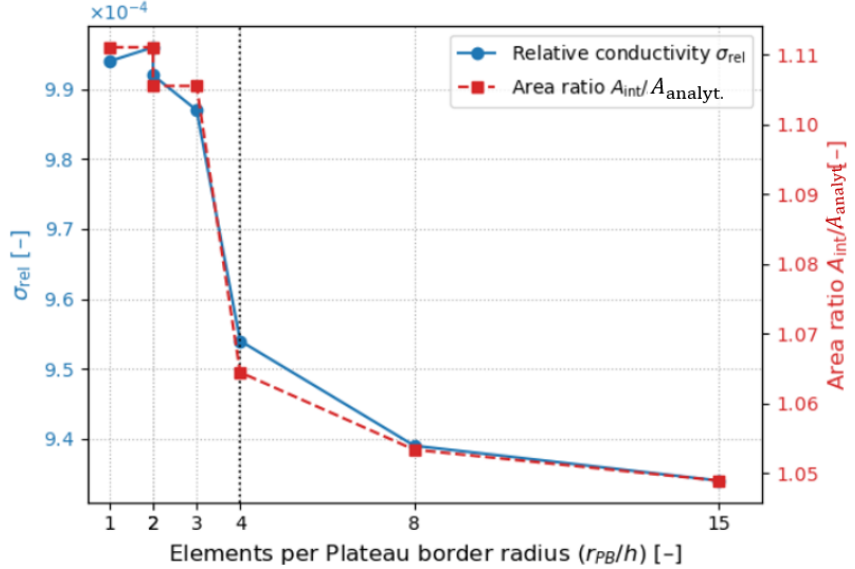


**Figure 3.8:** Refined triangular element ( $h$ -refinement) drawn in PowerPoint to present the idea of  $h$ . Specifying the maximum length of tetrahedra on faces or inside of objects. When the initial mesh has been generated, the refinement of triangle elements as per the  $h$  value will refine the initial mesh.

Sizes of  $h$  taken for single Plateau border vary from 0.05mm to 0.6 mm.

**Table 3.1:** Mesh convergence study on single Plateau Border (PB).

Mesh size [mm]	Area integral [m <sup>2</sup> ]	ANSYS current [I]	Analytical current [I]	$h/r_{PB}$	Number of Elments [I]	$\sigma_{\text{rel}}$
0.05	$9.44 \times 10^{-8}$	$6.23 \times 10^{-5}$	$6.00 \times 10^{-5}$	0.0646	15	0.000934
0.10	$9.48 \times 10^{-8}$	$6.26 \times 10^{-5}$	$6.00 \times 10^{-5}$	0.1291	8	0.000939
0.20	$9.58 \times 10^{-8}$	$6.36 \times 10^{-5}$	$6.00 \times 10^{-5}$	0.2582	4	0.000954
0.30	$9.95 \times 10^{-8}$	$6.58 \times 10^{-5}$	$6.00 \times 10^{-5}$	0.3873	3	0.000987
0.40	$9.95 \times 10^{-8}$	$6.61 \times 10^{-5}$	$6.00 \times 10^{-5}$	0.5165	2	0.000992
0.50	$1.00 \times 10^{-7}$	$6.63 \times 10^{-5}$	$6.00 \times 10^{-5}$	0.6456	2	0.000996
0.60	$1.00 \times 10^{-7}$	$6.64 \times 10^{-5}$	$6.00 \times 10^{-5}$	0.7747	1	0.000994



(a) Relative conductivity  $\sigma_{rel}$  (left axis) and ratio of area integral to analytical area versus elements per Plateau border radius.

**Figure 3.9:** Mesh convergence study on the single Plateau Border (PB): (a) percent deviation in current, and (b) stabilization of relative conductivity.

### Interpreted Results

Both quantities start to decrease beyond four elements per Plateau border radius; however, the values in Fig. 3.9 are mesh independent close to 15 elements per Plateau border radius. However, for further analysis, we have chosen four elements per Plateau border radius, and we will discuss the relevant reasons in a subsequent section.

### 3.3.2 Meshing strategy for Full Liquid Foam Geometry

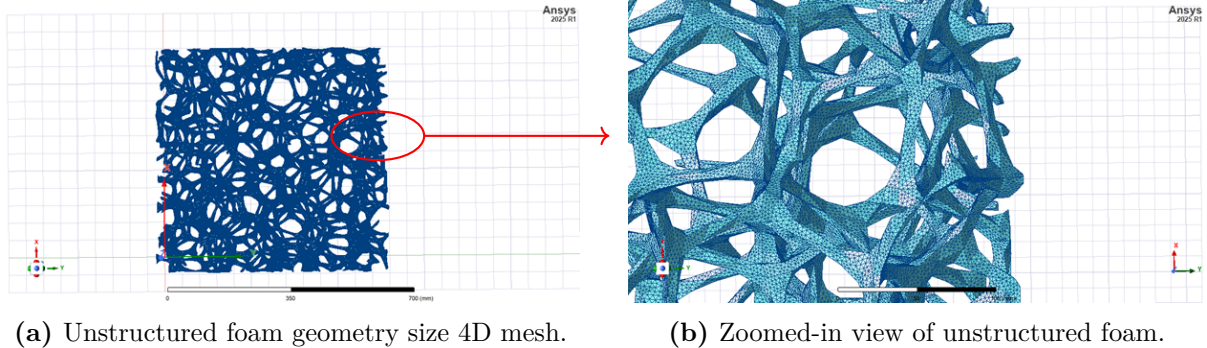
Based on the Single Plateau border study in the above Section, the Plateau border could be fully resolved with 15 elements per Plateau border radius, which represents an ideal case.

From the refinement ratio  $r_{pb}/h$ , it can be observed that as value of  $h$  decreases, the number of elements across the Plateau border radius increases linearly. For which the total element count scales cubically. Thus, the computational cost grows much faster than the geometric resolution. This agrees with classical discussions in isotropic mesh refinement studies, which suggest that isotropic mesh refinement (where each linear dimension of the element is divided by a factor of 2) in three dimensions, halving  $h$  in all three directions, creates approximately eight times more elements. More generally, the scaling follows  $N_{elements} \sim (1/h)^d$ , where  $d$  is the spatial dimension[39].

It was observed during the analysis stage for the choice of three elements per Plateau border for the whole foam geometry radius that the number of elements increased to approximately 10 million elements for the entire geometry after global adaptive passes of mesh refinement (adaptive mesh refinement) done by the solver. This consequently suggests choosing fifteen elements per Plateau border radius would have caused a considerably larger element growth rate for the whole liquid foam geometry. Hence, considering the above computational limitations, the choice of four elements per Plateau border radius, as interpreted from the analysis of a single Plateau border case, is the threshold

value where convergence was observed in the case of a single Plateau border.

In the Maxwell 3D solver, the computational domain is discretized using **tetrahedral elements**. This is the default by the solver while these elements are suitable for discretizing highly irregular and curved surfaces such as foam geometries.



(a) Unstructured foam geometry size 4D mesh.

(b) Zoomed-in view of unstructured foam.

**Figure 3.10:** Mesh visualization of foams: (a,b) unstructured foam with full mesh and zoomed region.

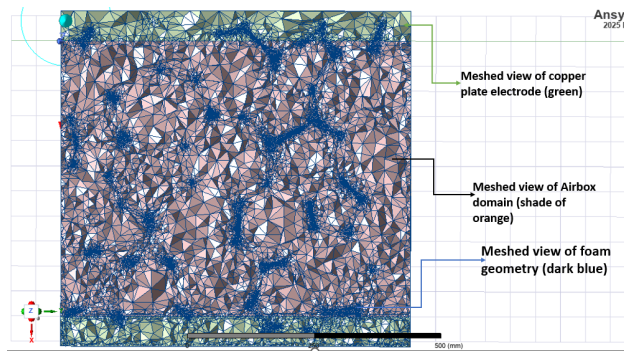


**Figure 3.11:** Meshed view of complete simulation domain.

## 3.4 PostProcessing

The conduction current was evaluated using multiple calculation ways to ensure accuracy and consistency.

- Extraction of current from the solved potential field
  1. **Ohmic loss integration.** The solver's ohmic loss density was integrated over the conducting volume as

$$P = \int_{V_{\text{foam}}} (\mathbf{E} \cdot \mathbf{J}) \, dV \quad (3.11)$$

The the above quantity the ohmic loss was used as below:

$$P = \text{Integrate}(\text{Volume}(pb\_Z), \text{Ohmic\_Loss}) .$$

2. **Convergence loss.** The current was also obtained directly from the solver's reported conduction loss given in watt which is power data as a global check, using

$$I = \frac{P}{\Delta V}, \quad (3.12)$$

Each of these methods yielded similar current values; hence, Ohmic loss values were chosen for further evaluation.

### 3.4.1 Validation Approach

The Validation is done against the well-established analytical models of conductivity, namely Feitosa, Lemlich, and Maxwell.

1. **Calculation of liquid fraction.** The liquid was determined from the geometry for the unstructured and structured case in all sizes from 1D to 4D. Using equation 3.5, liquid fractions were calculated for all sizes as follows:

The table below lists the liquid fraction  $\phi_l$  for the unstructured foam across sizes from 1D to 4D.

**Table 3.2:** Liquid fraction  $\phi_l$  (%) for the unstructured and structured foam by size.

Size	$\phi_l$ (%)
1D	2.54
2D	2.24
3D	2.20
4D	1.91
4D (structured)	5.53

2. **Model reference values.** At each computed liquid fraction  $\phi$ , the relative conductivity  $\sigma_{\text{rel}}$  was calculated using the analytical expressions from:
  - Lemlich model(Sec. 2.2.1),
  - Feitosa model(Sec. 2.2.3),
  - Maxwell model(Sec. 2.2.2).
3. **Comparison across cases.** For each meshing size (1D–4D) and each direction (X, Y, Z), the numerical values of  $\sigma_{\text{rel}}^{\text{num}}$  were compared directly against the model-predicted values  $\sigma_{\text{rel}}^{\text{model}}(\phi)$ . This provided a quantitative validation of the solver results across different discretizations and orientations. Consistent alignment across structured and unstructured cases, and across different mesh sizes that numerical procedure was successful.

# Chapter 4

## Results

### 4.1 Visualization of Results

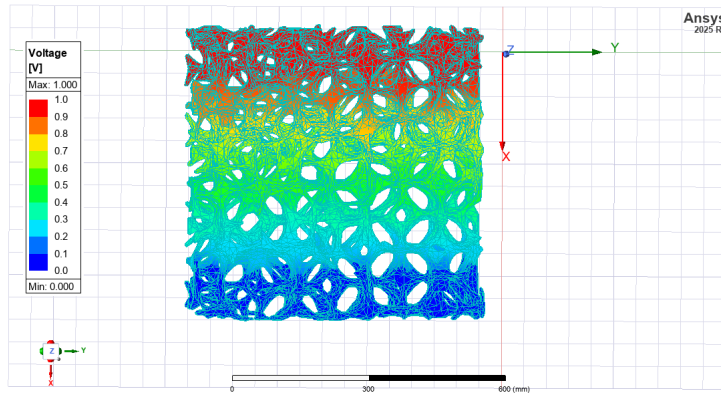


**Figure 4.1:** Voltage distribution across the structured foam simulation.

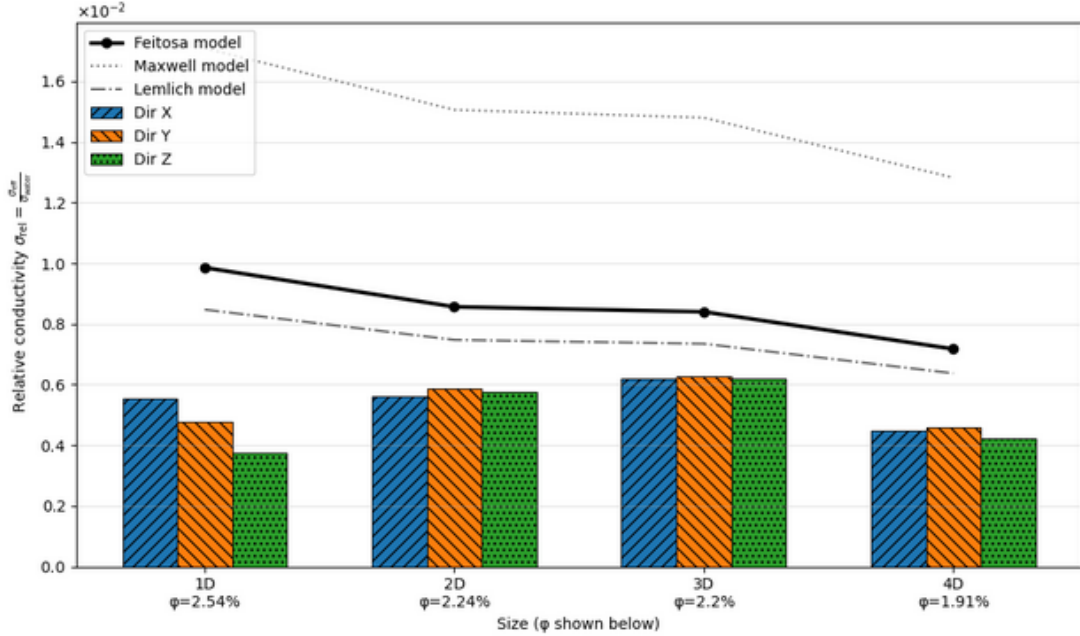
The Figure 4.1 shows the voltage distribution across the foam structure obtained from the DC conduction simulation in Ansys. A potential difference of 1 V was applied to the faces of the copper plates. The voltage decreases from the top plate (1 V) to the bottom plate (0 V), forming a nearly linear gradient along the vertical direction and indicating that the electric field is uniformly transmitted through the interconnected foam network.

#### 4.1.1 Unstructured Foam

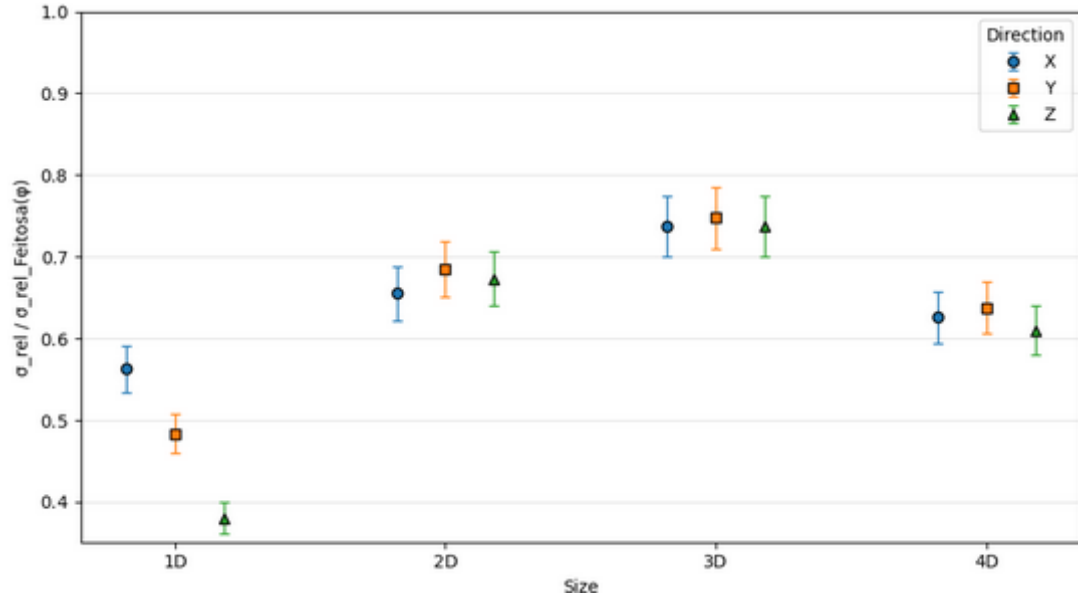
Simulations were conducted using Ansys Maxwell 3D for both structured and unstructured foam geometries. For the unstructured case, simulations were performed for sizes 1D, 2D, 3D, and 4D along the three principal directions ( $X$ ,  $Y$ , and  $Z$ ). For completeness and comparison, a structured foam case was also simulated at size 4D in the  $X$ ,  $Y$ , and  $Z$  directions. The plots below show the results for the unstructured foam.

For the relative conductivity  $\sigma_{\text{rel}}$  graph, we can see from the graph below that the relative conductivity increases with increasing liquid fraction, reaching its highest value at 3D. For 4D, the liquid fraction decreases by about 13%, yet the relative conductivity drops by nearly 28%. This means that only about half of the observed drop can be explained directly by the lower liquid fraction. With fewer mesh elements per Plateau border, the 4D case may not be as well resolved numerically, potentially introducing additional error in the conductivity calculation.

However, with increasing system size the directional dependency of relative conductivity decreases. At 1D size the difference between size directions is pronounced with variations up to 30–40%. By 3D the values converge within about 10%. At 4D, the three directions almost overlap within error bars and the difference is within 5%. This agrees with the observations of Weaire and Hutzler[37] that as the sample size increases, random foam geometries become effectively isotropic due to structural averaging over many cells.



(a) Relative conductivity of the unstructured foam along the  $X$ ,  $Y$ , and  $Z$  directions for sizes 1D–4D. Model predictions are shown as solid lines, calculated at the liquid fractions corresponding to each size. The main comparison is against the Feitosa model.



(a) Normalized relative conductivity of the unstructured foam as a function of size. The values are normalized by the Feitosa model prediction, i.e.,  $\sigma_{\text{rel}}/\sigma_{\text{rel\_feitosa}}(\phi)$ . Error bars represent the variability of relative conductivities for each size. Results for the  $X$ ,  $Y$ , and  $Z$  directions are shown separately to highlight anisotropy.

**Figure 4.3:** Conductivity analysis in unstructured foams: (a) relative conductivity and (b) normalized relative conductivity with error bars.

In the graph above, the relative conductivity  $\sigma_{\text{rel}}$  is compared against the relative conductivity calculated using the classical Feitosa model equation taken from (Sec. 2.2.3) as function of liquid fraction  $\phi$

Specifically chosen this form because it's a compact fit designed to work across a broad  $\phi$  range, as in this case. here,  $\sigma_{\text{rel\_feitosa}}$ , at the respective values of liquid fraction  $\phi$  for sizes ranging from 1D to 4D of unstructured foam.  $\sigma_{\text{rel\_feitosa}}$  removes the dependence on liquid fraction, as it differs between sizes, and focuses on size and directional effects. The error bar shows that for 1D, the mean ratio of relative conductivity rises to 0.48 and then to 0.74 for 3D, suggesting that convergence improves with domain size up to 3D, with a slight drop at 4D. Additionally, it can be seen that anisotropy is small for sizes 2D and 3D, but noticeably larger at 1D. All the ratios are below one, indicating that the model overpredicts the  $\sigma_{\text{rel}}$  values for given  $\phi$  values.

#### 4.1.2 Structured and Unstructured Comparison

##### Structured Foam

The graph below represents the relative conductivity for the Structured foam in each direction ( $X$ ,  $Y$ ,  $Z$ ); the values are well below the model's prediction of  $\sigma_{\text{rel}}$ .

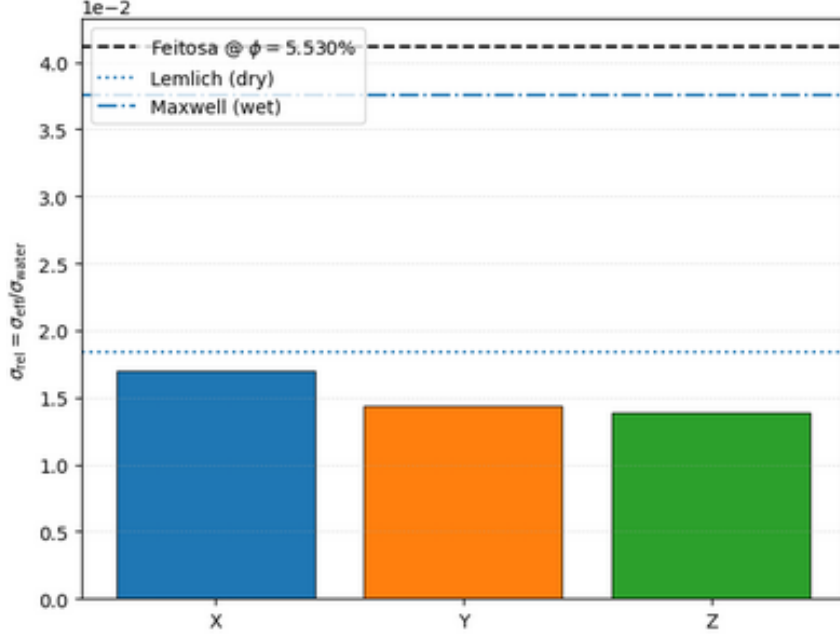


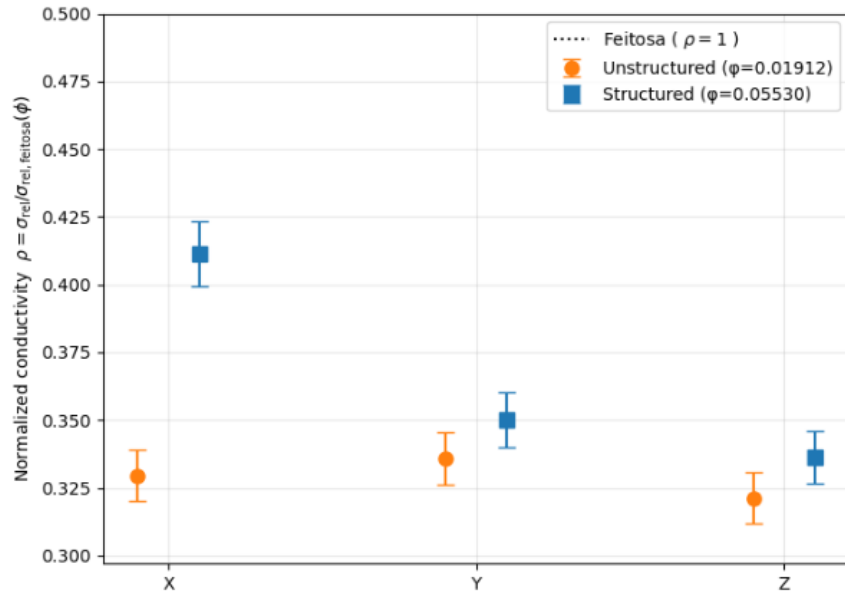
**Figure 4.4:** Directional relative conductivity  $\sigma_{\text{rel}}$  for the structured foam at  $\phi = 5.53\%$ , compared against classical models of Feitosa, Lemlich and Maxwell predictions.

Below graph shows Feitosa normalized relative conductivity  $\sigma_{\text{rel}}$  for structured and unstructured foam at their respective liquid fractions  $\phi_l$  for 4D structured its 5.503 percent and 4D unstructured its 1.911 percent geometries at size 4D across directions  $X$ ,  $Y$ , and  $Z$ . Classical Feitosa model equation taken from (Sec. 2.2.3) as function of liquid fraction  $\phi$

This equation is used to predict the relative conductivity at a given liquid fraction  $\phi$ , and then used for normalization by dividing the measured relative conductivity value:

$$\rho = \frac{\sigma_{\text{rel}}}{\sigma_{\text{rel\_feitosa}}(\phi)}. \quad (4.1)$$

All points lie below one, indicating that the model overpredicts conductivity values at a given  $\phi_l$ . For Structured foam, at  $\phi \approx 5.5\%$ , the relative conductivity values in all directions are well below Feitosa's model prediction. There is little difference observed in the  $Y$  and  $Z$  directions, which is well within or just above the expected numerical uncertainty. However, there is a deviation within the  $X$  direction reasonably large, but this is unlikely to reflect a genuine physical difference between structured and unstructured foam arrangements. Instead, the structured and unstructured samples were reconstructed and meshed separately, and any slight misalignment of the geometry, differences in boundary truncation, or mesh discretisation can produce an artificial bias in one direction.



(a) Percent difference  $\Delta(\%)$  between structured and unstructured foams after Feitosa normalization, with propagated error bars and a  $\pm 5\%$  uncertainty band.

**Figure 4.5:** Comparison of structured and unstructured foam conductivities at specific liquid fractions using Feitosa normalization.

# Chapter 5

## Discussion

The foremost statement to make here is that the Feitosa model over-predicts the relative conductivity values at the given specific liquid fractions for both structured and unstructured foam geometries.

That is mainly because the Feitosa model assumes infinite, homogenous, isotropic foam, perfect connectivity, and no contact resistance, but structured and unstructured foam geometry is created using the tool chain described in Chapter 3 from binarised tomography images. This will lead to having geometry which may have poorly connected Plateau borders, variation in thickness of Plateau borders, fewer conductivity pathways, hence the relative conductivity obtained after numerical simulation will always be comparatively lower.

### 5.1 Unstructured geometry

The focus of the work was to investigate the electrical conductivity of liquid foams, with a particular emphasis on the structure of foams. The results obtained through performing numerical simulations across different sizes and liquid fractions are compared to established models.

Firstly, as foam geometry sizes increase from 1D to 3D, the effective conductivity increases significantly and then drops, eventually overall, in all directions for 4D. Secondly, it clearly shows an increase in effective conductivity with an increase in liquid fraction. Hence, the 4D size, with a liquid fraction of  $\phi \approx 1.91\%$ , exhibits lower values of effective conductivity in all directions. This clearly confirms the Feitosa model[11], which attributes higher conductivity to higher liquid fraction. For 3D ( $\phi \approx 2.2\%$ ), we can see the highest liquid fraction. The outlier here is the 1D size despite having the highest liquid fraction, which falls below the Feitosa model, which could be attributed to the fact that the number of Plateau borders contributing to conduction is limited, the effective conduction path may be highly tortuous and sensitive to local effects, which reduces effective conductivity relative to the Feitosa model prediction. Another possibility could be a lack of structural averaging, which is more pronounced for larger geometries/systems (2D, 3D), as observed in the Feitosa model, which is based on experiments on bulk geometries where many cells contribute. The same phenomenon was observed by Weaire and Hutzler [27], who proved that a random foam structure requires a sufficient size to exhibit isotropy, with random variations averaging out to create more isotropic conduction paths.. However, for the 4D case of unstructured foam, the variation in relative conductivity is close to 4.4 percent, which is a small anisotropy; hence, it could be said

that the 4D case of unstructured foam geometry is isotropic.

### 5.1.1 Structured versus Unstructured Foam Geometry

The first thing to address while comparing structured and unstructured mesh geometry is the significant difference in the liquid fraction. Structured foam has a liquid fraction of 5.53%, compared to 1.91% for the unstructured case. After analyzing using both structured and unstructured mesh volumes, before and after remeshing, it can be stated that the structured mesh has nearly three times more mesh volume compared to the unstructured mesh.

Using the original mesh volumes (before remeshing), approximately 98% of the increase in liquid fraction can be attributed to the larger liquid volume of the structured mesh geometry. Remeshing changed the structured volume by +2.1% and the unstructured volume by -1.8%; hence, about 6% of the increase could be attributed to remeshing operations, as explained in Chapter 3. The small residual percentage (-4%) suggests that the structured case retains slightly less liquid fraction than expected from remeshed volume scaling, which is likely due to segmentation effects. Therefore, it can be concluded that the dominant factor is the larger liquid-holding geometry of the structured foam compared to the unstructured one.

Structured and Unstructured foam geometries were compared in order to assess whether topology influences electrical conductivity, and a comparison was made across three spatial directions. Possible reasons for X direction to be an outlier could be attributed to multiple factors, firstly, seemingly simple but important factor is that the foam-plate intersection can change for each direction based on way the geometry is meshed or on the way foam fits in airbox; that is defined as, the contact fraction, which can change with the direction even if you held the Airbox or copper plate electrode constant. Hence, if the contact fraction is more in the X direction, the conductivity could also be more by the same amount, which is a purely geometrical reason. Another possible attribute could be image pre-processing leading to meshing bias for example intensity normalization step which is stretching slices and doing that for each slice could lead to orientation artefacts; also, another possibility could global otsu thresholding can erode away features more along one axis, same goes with morphological cleanup and denoising per slice which leads to edges within slice are preserved better than edges across slices, hence when generating a finite element mesh from such images where Plateau border thickness differs by direction, reconstructed surfaces are more likely to be axis aligned as we are generating mesh out stack of images stack along particular direction, all of which might have tilted computed relative conductivity in x direction [15]. Hence, the *X*-direction outlier could be attributed to a numerical artefact since *Y* and *Z* directions show agreement within 5–8%.

### 5.1.2 Uncertainty and Sensitivity

In the present study, which assesses relative conductivity, due to limited computational resources available, it is important to account for other sources of uncertainties and factors for sensitivity in data.

As discussed previously in Chapter 3, the ideal simulation with a single Plateau border resolution was concluded using 10-15 elements across the Plateau border thickness. However, due to computational limitations, the present study was restricted to selecting four

elements for the whole liquid foam geometry (of course, geometry after remeshing), resulting in an under-resolved geometry that caused higher resistance and an underestimation of cross-sectional areas. This is also known as errors arising from geometric discretization, which refers to how well the mesh can represent curved and complex geometries, such as Plateau borders.

For an acoustic FEA formulation, the mesh must be sufficiently fine to minimize numerical dispersion effects resulting from finite discretization. Generally, the mesh should comprise at least ten low-order elements and five high-order elements per propagating or resonant wavelength of the material. A similar case study in COMSOL for a 90-degree circular arc was conducted, demonstrating that at least eight linear (first-order) elements per 90° arc are required to maintain an error of less than 1 percent[7].

Although these studies are not directly related to the present case of DC conduction in ANSYS Maxwell 3D , the idea of requiring at least 8-10 elements per Plateau border can be generalized for FEA solutions and provides a concrete reason for errors due to geometric discretization. Maxwell Solver in 3D conduction for the present study uses tetrahedral first-order (linear elements - straight edges, no curvature within elements). In the present study, using a 4-element resolution is insufficient; such under-resolution introduces an error of up to 30 percent, thereby biasing the conductivity.

Another contributing factor could be finite-size effects. In small volumes, percolating paths may be sparse or unevenly distributed across directions. This could lead to an overall increase in resistance along one axis, which could also be a reason we observe an X-direction outlier and a 1D size, despite having a high liquid fraction, resulting in low effective conductivity values. Local fluctuations in geometry or connectivity can significantly impact the results, even with a limited number of bubbles and Plateau borders.

Uncertainty could also be introduced during the preprocessing stage of raw grayscale images. In the case of image-based reconstructed liquid foam geometry, thresholding and binarization steps are necessary to segment liquid and gas phases, which can alter Plateau border connectivity, shifting the available conduction pathways. Also, morphological operations such as smoothing modify the thickness of the Plateau borders, which could change the calculated liquid fraction. In the present study, to make the mesh watertight and suitable for simulation, additional processing steps of Poisson reconstruction and isotropic remeshing were used. This remeshing results in a change in liquid foam volume.

In the case of the 4D Unstructured geometry, the volume reduction was about 9% from the original reconstructed geometry to the final remeshed geometry, which reduced the liquid fraction  $\phi_l$  by almost the same fraction. Since models such as Feitosa's are susceptible to the liquid fraction, this means the simulated  $\sigma_{\text{rel}}$  values could be  $\sim 9\%$  lower than what would be obtained from the original geometry. While such changes are more minor than those arising from limited mesh resolution, they still contribute to variability in parametric values, such as the liquid fraction  $\phi_l$  and the relative conductivity  $\sigma_{\text{rel}}$ .

# Chapter 6

## Conclusion and Future Work

In the present study, liquid foam geometries were reconstructed using the toolchain described in Chapter 3 from CT images obtained from Chammouma et al. [5] and simulated using the Numerical framework mentioned in Chapter 3. It can be concluded that the foam topology for 4D Unstructured foam does not significantly influence conductivity and appears to be isotropic.

Another possible approach to studying foam geometry could be to induce a pattern in a random foam structure. In a study done by Albuquerque & Fortes [1], they traversed vertical pin roads to impose geometric constraints on foam structure. 3D foams exhibited a periodic 3D structure (bubbles aligned and repeated along a certain direction) [1]. Such foams have apparent translational symmetry. Hence, the possibility to study engineered anisotropy and directional properties in foams.

Finally, considering computational aspects, with the availability of HPC clusters, it's possible to simulate larger foam geometries without remeshing or reducing the elements, thereby producing more accurate results.

# Bibliography

- [1] J. M. Albuquerque and M. A. Fortes, “Foam patterning by traversing pins,” *Philosophical Magazine A*, 2001. DOI: [10.1080/01418610108217145](https://doi.org/10.1080/01418610108217145).
- [2] S. Andrieux, A. Quell, C. Stubenrauch, and W. Drenckhan, “Liquid foam templating – a route to tailor-made polymer foams,” *Advances in Colloid and Interface Science*, 2018. DOI: [10.1016/j.cis.2018.03.010](https://doi.org/10.1016/j.cis.2018.03.010).
- [3] G. E. Archie, “The electrical resistivity log as an aid in determining some reservoir characteristics,” *Journal of Petroleum Technology*, 1942. DOI: <https://doi.org/10.2118/942054-G>.
- [4] I. Cantat et al., *Foams: Structure and Dynamics*, English, S. J. Cox, Ed., trans. by R. Flatman. Oxford, UK: Oxford University Press, 2013, ISBN: 9780199662890. DOI: [10.1093/acprof:oso/9780199662890.001.0001](https://doi.org/10.1093/acprof:oso/9780199662890.001.0001).
- [5] M. Chammouma, M. Jouanlanne, A. Egelé, D. Favier, J. Farago, and A. Hourlier-Fargette, “Crystalline structures in foams: Guided mechanical self-assembly of bubbles in fiber arrays,” *Journal of Physics: Materials*, 2025. DOI: [10.1088/2515-7639/adaa21](https://doi.org/10.1088/2515-7639/adaa21). [Online]. Available: [10.1088/2515-7639/adaa21](https://doi.org/10.1088/2515-7639/adaa21).
- [6] M. B. Clennell, “Tortuosity: A guide through the maze,” *Geological Society, London, Special Publications*, 1997.
- [7] COMSOL Blog. “Meshing considerations for linear static problems,” COMSOL AB, Accessed: Sep. 5, 2025. [Online]. Available: <https://www.comsol.com/blogs/meshing-considerations-linear-static-problems>.
- [8] A. K. Datye and R. Lemlich, “Liquid distribution and electrical conductivity in foam,” *International Journal of Multiphase Flow*, 1983. DOI: [10.1016/0301-9322\(83\)90112-X](https://doi.org/10.1016/0301-9322(83)90112-X).
- [9] W. Drenckhan and A. Saint-Jalmes, “The science of foaming,” *Advances in Colloid and Interface Science*, 2015. DOI: <https://doi.org/10.1016/j.cis.2015.04.001>.
- [10] S. Du, D. Li, M. J. Li, et al., “Numerical study on the effective thermal conductivity and thermal tortuosity of porous media with different morphologies,” *Science China Technological Sciences*, 2024. DOI: [10.1007/s11431-023-2481-4](https://doi.org/10.1007/s11431-023-2481-4).
- [11] K. Feitosa, S. Marze, A. Saint-Jalmes, and D. J. Durian, “Electrical conductivity of dispersions: From dry foams to dilute suspensions,” *Journal of Physics: Condensed Matter*, 2005. DOI: [10.1088/0953-8984/17/41/001](https://doi.org/10.1088/0953-8984/17/41/001).
- [12] L. J. Gibson and M. F. Ashby, *Cellular Solids: Structure and Properties*, 2nd ed. Cambridge, UK: Cambridge University Press, 1997, ISBN: 9780521499118. DOI: [10.1017/CBO9781139878326](https://doi.org/10.1017/CBO9781139878326). [Online]. Available: [10.1017/CBO9781139878326](https://doi.org/10.1017/CBO9781139878326).

- [13] Z. Huang et al., “A general patterning approach by manipulating the evolution of two-dimensional liquid foams,” *Nature Communications*, 2017. doi: 10.1038/ncomms14110.
- [14] J. D. Jackson, *Classical Electrodynamics*, 3rd ed. Wiley, 1999, ISBN: 9780471309321.
- [15] M. Jiang, I. Jasiuk, and M. Ostoja-Starzewski, “Apparent thermal conductivity of periodic two-dimensional composites,” *Computational Materials Science*, 2002. doi: 10.1016/S0927-0256(02)00234-3.
- [16] T. Jiang, H. Zhang, X. Zeng, C. Zhang, W. Gong, and L. He, “The effect of injection process for microcellular foaming on the cell morphology and surface quality of polyamide 6,” *Materials Research Express*, 2021. doi: 10.1088/2053-1591/abf8e3.
- [17] A. Jung, C. Redenbach, K. Schladitz, and S. Staub, *3d image based stochastic micro-structure modelling of foams for simulating elasticity*, Preprint, arXiv, 2025. doi: [arxiv.org/abs/2501.16194](https://arxiv.org/abs/2501.16194).
- [18] A. M. Kraynik, D. A. Reinelt, and F. van Swol, “Structure of random monodisperse foam,” *Phys. Rev. E*, vol. 67, p. 031403, 3 Mar. 2003. doi: 10.1103/PhysRevE.67.031403. [Online]. Available: <https://link.aps.org/doi/10.1103/PhysRevE.67.031403>.
- [19] J. Lamolinairie, B. Dollet, J.-L. Bridot, P. Bauduin, O. Diat, and L. Chiappisi, “Probing foams from the nanometer to the millimeter scale by coupling small-angle neutron scattering, imaging, and electrical conductivity measurements,” *Soft Matter*, 2022. doi: 10.1039/D2SM01252A.
- [20] V. Langlois, V. H. Trinh, and C. Perrot, “Electrical conductivity and tortuosity of solid foam: Effect of pore connections,” *Physical Review E*, 2019. doi: 10.1103/PhysRevE.100.013115.
- [21] R. Lemlich, “Theory for limiting conductivity of polyhedral foams,” *AIChE Journal*, 1978. doi: 10.1016/0021-9797(78)90339-9.
- [22] E. Lorenceau, N. Louvet, F. Rouyer, and O. Pitois, “Permeability of aqueous foams,” *European Physical Journal E*, 2009. doi: 10.1140/epje/i2008-10411-7.
- [23] E. B. Matzke, “The three-dimensional shape of bubbles in foam—an analysis of the role of surface forces in three-dimensional cell shape determination,” *American Journal of Botany*, 1946. doi: 10.2307/2437492. [Online]. Available: <https://doi.org/10.2307/2437492>.
- [24] J. C. Maxwell, *A Treatise on Electricity and Magnetism*. Clarendon Press, 1873, Reprinted by Dover, New York, 1954. [Online]. Available: <https://archive.org/details/electricitymagnetism01maxw>.
- [25] M. Mobarak, B. Gatternig, and A. Delgado, “On the simulations of thermal liquid foams using lattice boltzmann method,” *Energies*, 2022. doi: 10.3390/en16010195.
- [26] A. van der Net, A. Gryson, M. Ranft, F. Elias, C. Stubenrauch, and W. Drenckhan, “Highly structured porous solids from liquid foam templates,” *Colloids and Surfaces A: Physicochemical and Engineering Aspects*, vol. 346, no. 1-3, pp. 85–96, 2009. doi: 10.1016/j.colsurfa.2009.05.010.
- [27] R. Phelan, D. Weaire, E. A. J. F. Peters, and G. Verbist, “The conductivity of a foam,” *Journal of Physics: Condensed Matter*, 1996. doi: 10.1088/0953-8984/8/34/002. [Online]. Available: [h10.1088/0953-8984/8/34/002](https://doi.org/10.1088/0953-8984/8/34/002).

- [28] O. Pitois, N. Louvet, E. Lorenceau, and F. Rouyer, “Node contribution to the permeability of liquid foams,” *Journal of Colloid and Interface Science*, 2008. DOI: <https://doi.org/10.1016/j.jcis.2008.04.029>.
- [29] W. Research, *Electric currents*, <https://reference.wolfram.com/language/PDEModels/tutorial/Electromagnetics/ElectricCurrents.html>, Accessed: 2025-09-08, 2025.
- [30] W. R. Rossen and P. A. Gauglitz, “Percolation theory of creation and mobilization of foams in porous media,” *AICHE Journal*, 1990. DOI: [10.1002/aic.690360807](https://doi.org/10.1002/aic.690360807).
- [31] M. N. O. Sadiku, *Elements of Electromagnetics*, 5th ed. Oxford University Press, 2010, ISBN: 9780195300482.
- [32] A. Skrypnik, L. Knüpfer, P. Trtik, V. Tholan, S. Parkes, and S. Heitkam, “Neutron radiography of liquid foam structure near a vertical wall,” *Soft Matter*, 2023. DOI: [10.1039/D3SM00983A](https://doi.org/10.1039/D3SM00983A).
- [33] H. A. Stone, S. A. Koehler, S. Hilgenfeldt, and M. Durand, “Perspectives on foam drainage and the influence of interfacial rheology,” *Journal of Physics: Condensed Matter*, 2003. DOI: [10.1088/0953-8984/15/1/338](https://doi.org/10.1088/0953-8984/15/1/338).
- [34] R. Suman and D. Ruth, “Formation factor and tortuosity of homogeneous porous media,” *Transport in Porous Media*, 1993, Received 10 Feb 1992; Revised 22 Oct 1992; Issue Date Aug 1993. DOI: [10.1007/BF00616979](https://doi.org/10.1007/BF00616979). [Online]. Available: <https://doi.org/10.1007/BF00616979>.
- [35] S. Torquato, *Random Heterogeneous Materials: Microstructure and Macroscopic Properties*. Springer, 2002.
- [36] H. K. Versteeg and W. Malalasekera, *An Introduction to Computational Fluid Dynamics: The Finite Volume Method*, 2nd. Harlow, England: Pearson Education, 2007, ISBN: 978-0-13-127498-3.
- [37] D. Weaire and S. Hutzler, *The Physics of Foams*. Oxford, UK: Oxford University Press, 1999, ISBN: 9780198505518. DOI: [10.1093/oso/9780198505518.001.0001](https://doi.org/10.1093/oso/9780198505518.001.0001).
- [38] P. Yazhgur, C. Honorez, W. Drenckhan, D. Langevin, and A. Salonen, “Electrical conductivity of quasi-two-dimensional foams,” *Phys. Rev. E*, 2015. DOI: [10.1103/PhysRevE.91.042301](https://doi.org/10.1103/PhysRevE.91.042301).
- [39] O. C. Zienkiewicz, R. L. Taylor, and J. Z. Zhu, *The Finite Element Method: Its Basis and Fundamentals*, 7th ed. Oxford, UK: Butterworth-Heinemann, 2013, ISBN: 978-1856176330.